CHALMERS
UNIVERSITY OF TECHNOLOGY

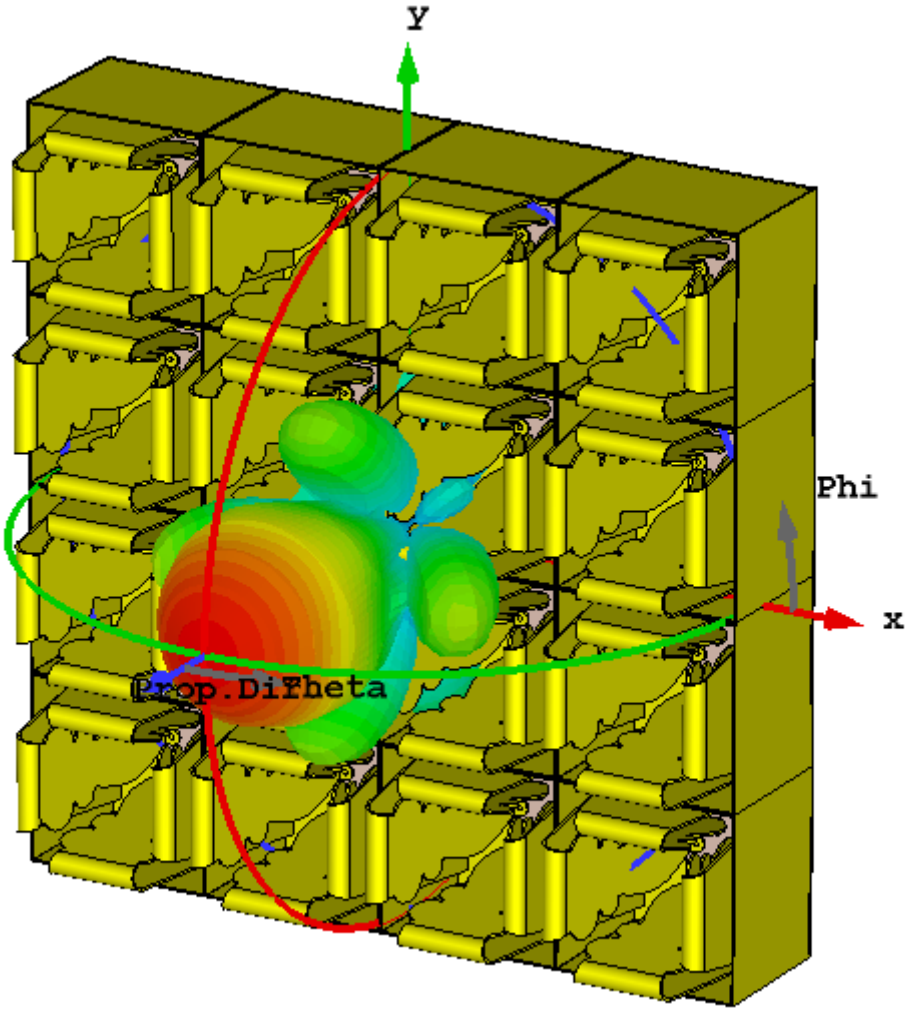

Design of a Dual-Polarized Phased Array with Self-Grounded Bowtie Antenna

Sub-6GHz Prototype

Master's thesis in Wireless, Photonics and Space

Samia Shafqaat

Department of Electrical Engineering
Master in Wireless, Photonics and Space Engineering
Gothenburg, Sweden, 2018

Design of a Dual-Polarized Phased Array with Self-Grounded Bowtie Antenna

Samia Shafqaat

Department of Electrical Engineering
Antenna Laboratory
Chalmers University of Technology

Design of a Dual-Polarized Phased Array with Self-Grounded Bowtie Antenna
SAMIA SHAFQAAT

E-mail: shafqaat@student.chalmers.se
Phone: +46 76 5775372

Supervisors: Ashraf Uz Zaman, Assistant Professor, Chalmers University of Technology, Department of Electrical Engineering, Sadegh Masouri Moaghddam PhD student at Electrical Engineering, Chalmers University of Technology, Esperanza Alfonso, Senior Antenna Designer, Gapwaves AB, Thomas Emanuelsson, CTO, Gapwaves AB.
Examiner: Jian Yang, Professor, Electrical Engineering, Chalmers University of Technology

Department of Electrical Engineering
Chalmers University of Technology
SE-412 96 Gothenburg
Telephone +46 31 7721000

Gapwaves AB
Banehagsgatan 22
SE-414 51 Gothenburg
Telephone +46 31 762 60 40

Cover: 2D- Far-field radiation pattern of the 4×4 array in broadside scanning at the frequency 4.8 GHz. The directivity of the main beam is 17.4 dBi and side lobe level is at -12.9 dB.

Gothenburg, Sweden 2018

Design of a Dual-Polarized Phased-Array with Self-Grounded Bowtie Antenna
SAMIA SHAFQAAT
Department of Electrical Engineering
Chalmers University of Technology

ABSTRACT

Phased Array antennas are one of the key components of the system design in the 5G wireless technology. They have many attractive benefits to offer in Sub-6 GHz for MIMO technology. The main benefit is their ability to directionally steer the main beam with the help of the electronic phase shifters without mechanically re-positioning the individual antennas.

In this report the design, optimization and simulation results of a dual-polarized phased-array self-grounded bowtie antenna is discussed. A detailed literature study has been performed on the basic concepts of antenna. Moreover, published papers for the self-grounded bowtie antenna have been analysed for a deeper understanding of the working principles of the self-grounded bowtie antenna. Different modelling techniques were studied and applied on the design of the single element to achieve the desired performance.

A compact wide-band, *4 by 4* dual-polarized phased-array self-grounded bowtie antenna has been designed and analyzed for the bandwidth of 3.1-4.8 GHz, with the aim to manufacture a prototype. For broadside direction, the array has a directivity of 14.3-17.8 dBi and a reflection co-efficient better than -15 dB for the entire bandwidth. For scanning up to ±30°, the elements in the middle of the array have reflection co-efficient better than -10 dB for the bandwidth of 3.1-4.7 GHz in both E-and H-plane. For scanning up to ±45° the middle elements have reflection co-efficient better than -10 dB for the bandwidth 3.1-4 GHz in E-plane and in H-plane. Almost all elements have reflection coefficient better than -8 dB for the bandwidth 3.3-3.6 GHz.

For scanning up to ±60°, almost all elements have a reflection co-efficient better than -8dB for the frequency band 3.2- 3.5 GHz in E-plane and only the corner elements (elements:1, 13, 16 and 4) had a reflection co-efficient better than -8dB for a frequency band of 3.36-4.85 GHz in H-plane. The grating lobes appear only when scanning for ±60 ° for frequencies higher than 4.2 GHz.

In conclusion, the array has a good performance for main beam steering up to ±45°. A prototype is under the process to be manufactured to show promising performance and a potential place in the market for wideband phased array antennas.

Keywords: Phased-array, dual-polarized, Bowtie, Self-grounded Bowtie antenna, beam-scanning.

ACKNOLOWDGEMENTS

This thesis work was a joint ventured of Antenna Systems Group at Electrical Engineering Department, Chalmers University of Technology and Gapwaves AB. It was conducted at the both places and was sponsored by Gapwaves AB. The examiner for this project was Jian Yang, Professor at Chalmers. The supervisors from Chalmers were Ashraf Uz Zaman, Assistant Professor and Sadegh Masouri Moaghddam, a PhD student at Electrical Engineering. From Gapwaves, Esperanza, Senior Antenna Engineer and Thomas Emmanuelson, CTO Gapwaves were supervising the project.

I would like to express my gratitude to Gapwaves AB and Chalmers, for providing me with this thesis work opportunity. I would like to thank my examiner and all supervisors for their dedicated supervision. This has been a learning experience of practical antenna engineering.

I would like to dedicate this work to my husband, Muhammad Ahmed for his constant motivation and my daughter Inaya Ahmed.

Samia Shafqaat, Gothenburg, June 2018

Contents

List of Figures xi
List of Tables ..... **Error! Bookmark not defined.**
1 INTRODUCTION 16
1.1 Aim of the project 16
2 LITERATURE STUDY 17
2.1 Antennas 17
2.1.1 Different Antenna types and Uses 17
2.2 Basic Antenna Concepts 18
2.2.1 Far-Field Distance and Radiation 18
2.2.2 Polarization of the Radiation Fields 18
2.2.3 Radiation Pattern 19
2.2.4 Directive Gain and Beam Width 20
2.2.5 Theory of Linear Array Antennas 21
2.2.6 Steering Main Beam and Grating Lobes 22
2.2.7 Aperture Efficiency, Directivity and Affective Area 22
2.2.8 Electrical length of Antenna 23
2.3 Modeling Techniques 23
2.3.1 Inductive and Resistive Loading 23
2.4 Ultra-Wide Band Wireless Technology and Self-Grounded Bowtie Antenna 24
2.4.1 UWB Advantages and Applications 24
2.4.2 UWB Antennas 24
2.5 Self-Grounded Bowtie Antenna 26
3 SINGLE ELEMENT DESIGN AND SIMULATION 27
3.1 Designs Specifications 27
3.1.1 Bandwidth 27
3.1.2 Element Spacing and Beam Scanning of the array antenna 27
3.1.3 Number of ports and Polarizations 28
3.1.4 Elements Isolation 28
3.1.5 Polarization Isolation 28
3.1.6 Directivity 28
3.1.7 Easy Manufacturing 28
3.2 Element Modelling and Design 30

3.2.1 Element Dimensions 31
3.2.2 Element Spacing 32
3.2.3 Height of the Element 32
3.2.4 Shape of the Petals of the Element 32
3.2.5 Boundary Walls of the Single Element 33
3.2.6 Feeding and Ports of the Element 34
3.2.7 Ground Plane of the Element 34
3.3 Single Element Simulation Results 35
3.3.1 Single Element Broadside Radiation 35
3.3.2 Single Element Main Beam Scanning up to $\pm\mathbf{30}°$, $\pm\mathbf{45}°$ and $\pm\mathbf{60}°$ in E- and H-planes. 37
4 ARRAY DESIGN AND SIMULATION RESULTS 40
4.1.1 Broadside Radiation of the Array: 41
4.1.2 Directivity, Grating lobes and Side-lobe Levels of the Array in Broadside Direction 42
4.1.3 Individual Port Reflection Co-efficient of Elements in the Array in Broadside Direction 42
4.1.4 Combined Reflection Co-efficient of Individual Elements in the Array in Broadside Direction 43
4.1.5 2-Port Network of the Array Antenna 44
4.2 Array Main Beam Scanning up to $\pm\mathbf{30}°$, $\pm\mathbf{45}°$ and $\pm\mathbf{60}°$ in E- and H-planes for One Polarization 45
4.2.1 Directivity, Grating lobes and Side-lobe Levels of the Array for Main Beam Scanning in E- and H-planes 45
4.2.2 Individual Port Reflection Co-efficient of Elements in Array for Scanning up to $\pm\mathbf{30}°$ in E-plane 46
4.2.3 Combined Reflection Co-efficient of Individual Elements in Array for Scanning up to $\pm\mathbf{30}°$ in E-plane 47
4.2.4 Individual Port Reflection Co-efficient of Elements in Array for Scanning up to $\pm\mathbf{45}°$ in E-plane 48
4.2.5 Combined Reflection Co-efficient of Individual Elements in Array for Scanning up to $\pm\mathbf{45}°$ in E-plane 49
4.2.6 Individual Port Reflection Co-efficient of Elements in Array for Scanning up to $\pm\mathbf{60}°$ E-plane 50
4.2.7 Combined Reflection Co-efficient of Individual Elements in Array for Scanning up to $\pm\mathbf{60}°$ in E-plane 51
4.2.8 Far-Field Plots of the Array in E-plane: 52

4.2.9 Individual Port Reflection Co-efficient of Elements in Array for Scanning up to ±30° in H-plane....53
4.2.10 Combined Reflection Co-efficient of Individual Elements in Array for Scanning up to $\pm\mathbf{30}°$ in H-plane....54
4.2.11 Individual Port Reflection Co-efficient of Elements in Array for Scanning up to $\pm\mathbf{45}°$ in H-plane....55
4.2.12 Combined Reflection Co-efficient of Individual Elements in Array for Scanning up to $\pm\mathbf{45}°$ in H-plane....56
4.2.13 Individual Port Reflection Co-efficient of Elements in Array for Scanning up to ±60° in H-plane....57
4.2.14 Combined Reflection Co-efficient of Individual Elements in Array for Scanning up to ±60° in H-plane....58
4.2.15 Far-Field Plots of the Array in H-Plane:....59
5 DISSCUSSION....60
5.1 Further Improvements and Future Work....60
5.2 Potential Applications....61
5.3 Conclusion....62

List of Figures

Figure 2.1 Far-field radiation pattern in the Cartesian co-ordinate system showing directivity as a function of phi in theta=90 plane. The main lobe level at 8.03 dBi and side lobe level at -5 dBi. 20
Figure 3.1 Single Element Design (a) with boundary walls, (b) without boundary walls 30
Figure 3.2 Element Geometry and Dimensions 31
Figure 3.3 Single element structure showing the minimum gap between the petals 33
Figure 3.4 (a) Reflection co-efficient when we simultaneously excite the opposite ports with differential excitation of single element in periodic boundary conditions (b) Isolation between the polarizations for differential excitation of the ports of the single elements 35
Figure 3.5 Far-field Cartesian plot for broadside radiation of the single element. 36
Figure 3.6 Single element directivity plot for an array (4× 4) for broadside radiation. 36
Figure 3.7 Reflection Coefficient for different scanning of the single element in(a) E- and (b) H-plane. 38
Figure 3.8 Directivity plot for an array (4× 4) for broadside direction and scanning up to ±30°, ±45° and ±60° in E- and H-plane. 38
Figure 3.9 Far-field plots of the single element in infinite periodic boundary condition for different scanning's for frequencies (a) & (b) 3.2 GHz, (c) & (d) 4 GHz and (e) & (f) 4.8 GHz in E- and H-planes respectively. 39
Figure 4.1 Front view the array design in CST 40
Figure 4.2 Directivity plot of the array in broadside direction. 42
Figure 4.3 Reflection co-efficient of ports 2, 4,6 and 8 in the array for broadside direction .. 42
Figure 4.4 Reflection co-efficient of ports in the array 18,20,30 and 32 for broadside direction 43
Figure 4.5 Combined reflection co-efficient of the ports for elements 1, 2, 5 and 6 for broadside direction. 43
Figure 4.6 2-port S-parameters for broadside scanning for the array antenna 44
Figure 4.7 Directivity plot of the array for broadside direction and main beam scanning up to ±30°, ±45° and ±60° in E- and H-planes 46
Figure 4.11 Reflection co-efficient of ports 2, 4,6 and 8 in the array for scanning up to ±30° in E-plane 46

Figure 4.12 Reflection co-efficient of ports 18,20,30 and 32 in the array for scanning up to ±30° in E-plane 47
Figure 4.13 Combined reflection co-efficient of the ports of the elements 1, 2, 5 and 6 in the array for scanning ±30° in the E-plane 47
Figure 4.16 Reflection co-efficient of ports 2, 4,6 and 8 in the array for scanning up to ±45° in E-plane 48
Figure 4.17 Reflection co-efficient of ports 18,20,30 and 32 in the array for scanning up to ±45° in E-plane 48
Figure 4.18 Combined reflection co-efficient of the ports for elements 1, 2, 5 and 6 in the array for scanning up to ±45° in E-plane 49
Figure 4.21 Reflection co-efficient of ports 2, 4,6 and 8 in the array for scanning up to ±60° in E-plane 50
Figure 4.22 Reflection co-efficient of ports 18,20,30 and 32 in the array for scanning up to ±60° in E-plane 50
Figure 4.23 Combined reflection co-efficient of the ports for elements 1, 2, 5 and 6 for scanning up to ±60° in E-plane 51
Figure 4.24 Far-field plots of the array for broadside radiation and scanning up to ±30°, ±45° and ±60° in E-plane for frequencies (a) 3.2 GHz (b) 4 GHz (c) 4.8 GHz. 52
Figure 4.27 Reflection co-efficient of ports 2, 4,6 and 8 for scanning up to ±30° in H-plane 53
Figure 4.28 Reflection co-efficient of ports 18,20,30 and 32 for scanning ±30°in H-plane ..53
Figure 4.29 Combined reflection co-efficient of the ports for elements 1, 2, 5 and 6 for scanning up to ±30° in H-plane 54
Figure 4.32 Reflection co-efficient of ports 2, 4,6 and 8 scanning up to ±45° in H-plane.....55
Figure 4.33 Reflection co-efficient of ports 18,20,30 and 32 scanning up to ±45° in H-plane 55
Figure 4.34 Combined reflection co-efficient of the ports for elements 1, 2, 5 and 6 for scanning up to ±45° in H-plane 56
Figure 4.37 Reflection co-efficient of ports 2, 4,6 and 8 for scanning up to ±60° in H-plane 57
Figure 4.38 Reflection co-efficient of ports 18,20,30 and 32 for scanning up to ±60° in H-plane 57

Figure 4.39 Combined reflection co-efficient of the ports for elements 1, 2, 5 and 6 for scanning up to ±60° in H-plane.....58
Figure 4.40 Far-field plots of the array for broadside radiation and scanning up to ±30°, ±45° and ±60° in H-plane for frequencies (a) 3.2 GHz (b) 4 GHz (c) 4.8 GHz.....59

List of Tables

Table 3-1 Dimensions of the Element 31
Table 4-1 Dimensions of the array.....40
Table 4-2 Front view of the 4x4 array showing symmetry for reflection co-efficient for broad scanning for one polarization.....41
Table 4-3 Phase difference $\Delta\phi$ for different beam scanning.....45

1 INTRODUCTION

With the development of 5G technology on the way, new chapters unfold for the wireless networks. 5G has a lot to offer in technology which paves the way for many advanced applications. 5G is about higher data rates, efficient spectrum utilization, lower energy consumption, higher bandwidths, greater capacity and security and so many other things.

It is becoming understandable that the frequencies between 30 GHz-300GHz, also known as the millimeter-waves frequencies will become the frequency band for 5G network. But many problems are needed to be taken care of while working on the millimeter waves especially for the high coverage. For instance, signal attenuation is quite high due to atmospheric absorption for these frequencies and rain and fog attenuates the signal, thus reducing the range of the signal. Other than that, millimeter signals are easily scattered by the rain droplets, as they are roughly the same size as the mm wavelength. Hence many problems need to be solved for the millimeter.

Whereas, frequencies under the 6GHz provides an alternative over the millimeter-waves for 5G networks. Although less spectrum is available for sub-6GHz, but the MIMO technology along with many antennas can solve many problems. In MIMO technology interference is minimalized and it can accommodate many users at the same time with the added benefit of higher date rates. It is believed that the MIMO technique can provide date rates higher than 1 Gps [1]. With multiple antennas transmitting data at the transmitter end and with multiple antennas at the receiver end to receive, one can make use of the limited radio frequency spectrum.

This calls for the need for phased array antennas for 5G MIMO technology. Phased array antennas provide directive beam forming without compromising the gain and bandwidth. The combination of ultra-wide band antennas with MIMO technique can provide the benefits of both, that is high data rates and a very wide frequency band in 5G.

1.1 Aim of the project

In this project, a sub 6GHz self-grounded bowtie phased array antenna is designed for a 5G MIMO network. The aim is to design, fabricate and analyze the phased array self-grounded antenna for sub-6GHz, with the aim to manufacture a prototype. However due to time constraint this report only contains the results corresponding to the simulations, as the prototype had not been manufactured yet.

This report is divided into four main parts: First part is the detailed study of the basic concepts of the antenna, different UWB antennas, the self-grounded bowtie antenna and some useful modeling techniques are discussed a well. The second part has the design and the structure of the single element and the simulation results for the single element. In the third part simulation results of the array antenna are discussed. The fourth part has discussions and further improvements of the design and a few recommendations on future work.

2 LITERATURE STUDY

This chapter contains a detailed literature study of some basic concepts of antenna. Different antenna types are mentioned and UWB antennas are discussed. Published papers for self-grounded bowtie antennas were conferred. Moreover, some modelling techniques that proved beneficial while designing and optimizing the element design are also mentioned.

2.1 Antennas

Antenna is a device which can receive and transmit electromagnetic signals from a system design to free space and vice versa. It acts as a directional filter in free space for electromagnetic waves [2]. In a wireless network system, antenna is an important block of the receiver and the transmitter. It is a transducer which converts the electromagnetic wave energy which it receives from the free space into alternating electric current.

2.1.1 Different Antenna types and Uses

Antennas are used in wireless telecommunication ground stations for point-to-point radio links, direct broadcast, local area network, mobile telephony, traffic tolls systems and navigation. They are also use in satellite wireless communication for providing communication with other satellites and with earth stations for different purposes such as broadcasting satellite TV signals, transmission of data between earth stations and different satellites. They are also used in handheld mobile systems such as mobile phones, moving vehicles etc. These days antennas are used in different radar applications in military as well as civilian. One example of airborne and space borne radar is Synthetic Aperture Radar, SAR, which can generate electronically larger antenna than the physical one for its high-resolution image processing [2].

Many different types and variations of Antenna exist for many different applications. We have wire antennas which include dipoles, monopoles, loops and Yagi Uda. These antennas have low gains and used for lower frequencies. They have an advantage of being low in weight and cost. Other than that, we have aperture antennas like horn and waveguide antennas. Aperture antennas are mostly used at millimeter-waves and microwaves frequencies and have moderate gains. Reflector antenna like corner and parabolic reflector and lens antennas can be categorized as aperture antennas. Third category of antenna is of printed antennas which include patch antennas, microstrip patch antennas, printed slots and dipoles on a substrate. These antennas can be tapered or arrayed to have high gains and mostly used for millimeter-waves and microwaves frequencies. Bowtie and log periodic dipole array are log periodic antennas, which have high gains and wide bandwidths. Recent works have been done on dielectric resonator antenna and frequency independent antennas [2] [3] [4].

An array of antennas can be made with two or more antenna elements with a feed network. It is possible to achieve better performance than the single antenna element as we can get higher directivity and gain with array antennas [2]. Which will be discussed more in Section 2.2.5. Many different form of array antenna exist such as linear, planar or conformal. Single and multibeam forming and steering and sidelobe levels can be controlled by the feed network of the array antenna.

2.2 Basic Antenna Concepts

This section covers some basic antenna concepts that were used throughout the project.

2.2.1 Far-Field Distance and Radiation

The antenna is usually needed to transfer signals at large distances in the far field region, where the electromagnetic waves radiating spherically away from the antenna appear as plan waves. In the far-field distance, the wave-front of the spherical radiated waves of the antenna become close to phase-fronts of a plan wave and the near-fields of antenna become negligible. This approximation depends on the maximum dimension D of the antenna and the wavelength and can be expressed as [2] [3],

$$r = \frac{2D^2}{\lambda} m \tag{2-1}$$

The radiated electric field in the far field distance of an arbitrary antenna placed in the origin of the spherical coordinate system can be expressed as [2] [3],

$$\bar{E}(r,\theta,\phi) = \bar{G}(\hat{r})\frac{1}{r}e^{-jk_0 r} = \bar{G}(\theta,\phi)\frac{1}{r}e^{-jk_0 r} \quad \frac{V}{m} \tag{2-2}$$

Where $\bar{G}(\theta,\phi)$ is the complex far-field function or the radiation field function in the spherical co-ordinate system. $\bar{E}$ is the vector notation of the electric-field and $k_0 = {}^{2\pi}/_{\lambda}$ is the propagation constant of the wave in the free-space. $\hat{\theta}$ and $\hat{\phi}$ are unit vectors of the spherical coordinate system and r is the radial distance from the origin. The electric field radiate away from the antenna in the radial direction, with an amplitude variation of ${}^{1}/_{r}$ and phase variation of $e^{-jk_0 r}$.

$$\hat{r} = x\hat{x} + y\hat{y} + z\hat{z}, \qquad r = \sqrt{x^2 + y^2 + z^2} \quad \text{and} \quad \hat{r} = \mathbf{r}/r \tag{2-3}$$

The magnetic field can be calculated form the electric field [4]

$$\bar{H}(r,\theta,\phi) = \frac{1}{\eta_0}\hat{n} \times \bar{E}(r,\theta,\phi) \tag{2-4}$$

2.2.2 Polarization of the Radiation Fields

The time-harmonic E-and H-fields of the plane wave propagate along the positive z-direction and have components in x- and y-direction E_x , E_y $H_x$and H_y. We can modulate different signals on these components on the same frequency and make use of the frequency more effectively. The receiving or transmitting antennas also need to be polarized accordingly and need to have good isolation between different polarization to receive and transmit signals of different polarizations [2]. The antenna can be dual polarized. Meaning that on the same frequency we can modulate different signals on the two E-field components in the x-and y-direction.

The polarization of the plane wave is always defined by the direction of the electric field only. It is the trace made by the tip of the electric-field of the electromagnetic wave as it propagates on the plane perpendicularly to the direction of the propagation. Plane waves can be polarized

linearly, circularly and elliptically. When E-field is parallel to the y-axis or x-axis, the plane wave is linearly y-polarized and x-polarized respectively.

The total electric- and magnetic fields can be expressed in its x- and y-components, [2]

$$\overline{E} = E_t e^{-jkz} = \left[E_x \hat{x} + E_y \hat{y}\right] e^{-jkz} \quad \text{and} \quad \overline{H} = -\frac{1}{\eta}\left[E_y \hat{x} + E_x \hat{y}\right] e^{-jkz} \tag{2-5}$$

Electric field can be expressed into its co-polar component E_{co} and cross-polar component E_{xp}, which are parallel to the unit vectors $\widehat{\boldsymbol{co}}$ *and* $\widehat{\boldsymbol{xp}}$ respectively. These unit vectors are orthogonal to the unit vector $\hat{z}$. One of the component is treated as the desired component and the other as undesired component. The co-polar component is usually treated as the desired component and cross-polar as undesired component [2]. The co- and cross-polar component of the E-field can be calculated by the scalar multiplication with $\widehat{\boldsymbol{co}}$ and $\widehat{\boldsymbol{xp}}$ respectively,

$$E_{co} = E_t . \widehat{\mathbf{co}}^*, \quad E_{xp} = E_t . \widehat{\mathbf{xp}}^* \quad \text{and} \quad \overline{E} = \left[E_{co}\widehat{\mathbf{co}} + E_{xp}\widehat{\mathbf{xp}}\right] e^{-jkz} \tag{2-6}$$

When the E-field is linearly y-polarized, the co- and cross-polar E-field components are,

$$\widehat{\mathbf{co}} = \hat{y}, \quad \widehat{\mathbf{xp}} = \hat{x} \tag{2-7}$$

$$E_{co} = E_t . \hat{y}^* = E_y \tag{2-8}$$

$$E_{xp} = E_t . \hat{x}^* = E_x \tag{2-9}$$

Similarly, when the E-filed is linearly x-polarized, the co- and cross-polar E-field components are

$$\widehat{\mathbf{co}} = \hat{x}, \quad \widehat{\mathbf{xp}} = -\hat{y} \tag{2-10}$$

$$E_{co} = E_t . \hat{x}^* = E_x \tag{2-11}$$

$$E_{xp} = -E_t . y^* = -E_y \tag{2-12}$$

2.2.3 Radiation Pattern

It is the plot of the magnitude of the far-field strength versus the angular position around the antenna at a fixed distance [3]. Radiation patterns can be omnidirectional, directional and isotropic depending on the antenna. Many other radiation patterns exist. For examples Radars have crescent shape beams. Antennas with pencil-shaped beams have narrow beams and low side lobes. Omni directional antennas have doughnut shaped beams and are ideal for connecting to devices that are on the same plane or to either side of each other.

The graphical representation of the co-polar far-field function is of interest and it can be represented in polar, rectangular and 3D form with the magnitude of the far-field function expressed in dB, as a function of polar angle or theta θ for a φ plane or for φ in the polar(theta) plane [2].

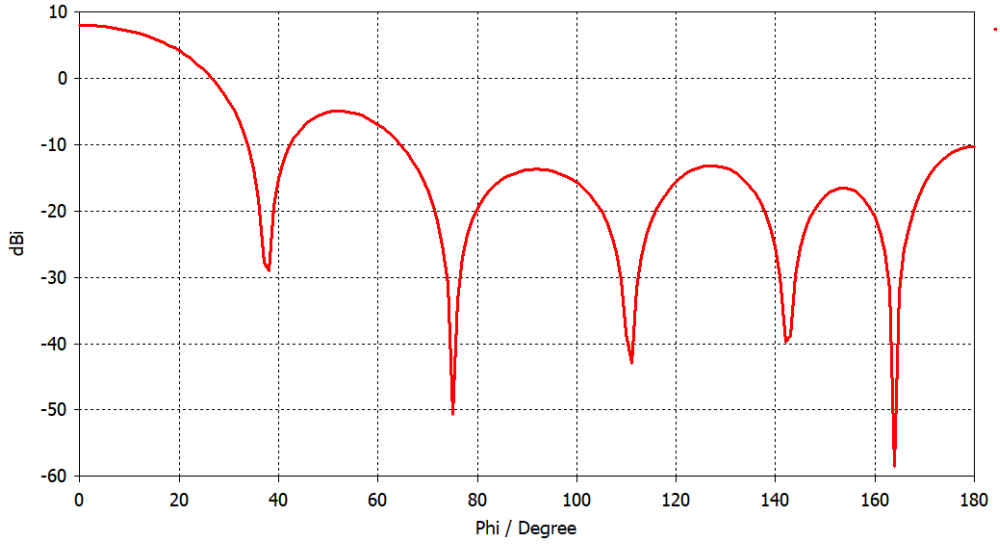

Figure 2.1 Far-field radiation pattern in the Cartesian co-ordinate system showing directivity as a function of phi in theta=90 plane. The main lobe level at 8.03 dBi and side lobe level at -5 dBi.

Radiation pattern consists of main lobe called the main beam, nulls and many side lobes usually lower in magnitude than the main beam. They are always normalized to the level on the axis $\theta = 0$ [2].

$$(G_{co}(\theta,\phi))_{dB} = 10log\left|\frac{G_{co}(\theta,\phi)}{G_{co}(0,\phi)}\right|^2 dB \tag{2-13}$$

2.2.4 Directive Gain and Beam Width

Directive gain is the ability of an antenna to focus power in a given direction. Antenna's far-field function are normalized to the isotropic levels G_{ISO} by the total radiated power and expressed in dBi (relative to the isotropic level) and are called as the directive gain of the far-field function. The directive gain of the co-polar far-field function is defined as,

$$(D_{co}(\theta,\phi))_{dB} = 10log\frac{|G_{co}(\theta,\phi)|^2}{|G_{ISO}|^2} dBi \tag{2-14}$$

Where the G_{ISO} isotropic radiation is the radiation from the point source and it radiates uniformly in all directions with the same intensity regardless of the direction of the measurement. And it is defined from the co-polar component of the far-field radiation function.

Whereas, the directivity is the value of the gain in the center beam of the far-field radiation pattern and for the centered beams it is given at $G_{co}(0,0)$.

Beam width is the width of the main beam of the antennas radiation patterns. Many antennas have narrow beam width meaning that they transmit power over small angular distance. Such antennas have high directivity. While some have wider main beam width and they can transmit power to a wider angular region. They have low directivity. Each of these antennas have their own applications. Often the term 3dB beam width is used to express antennas focusing ability and it's the angular width of the main beam where the power has dropped to 3 dB from its maximum value at $\theta = 0^{\circ}$. It is also called the half-power beam width.

2.2.5 Theory of Linear Array Antennas

Two or more than antennas elements can be arranged into a straight line making a linear array. Planar arrays can be think of linear arrays of many linear arrays. Theory of linear array is also applicable to planar array. The Array antenna systems have many benefits over single antennas. The Far-field function of the array with equal and same orientated elements can be actually found by the product of element factor and array factor.

$$\mathbf{G_A}(\hat{\mathbf{r}}) = \mathbf{G}(\hat{\mathbf{r}})\mathrm{AF}(\hat{\mathbf{r}}) \tag{2-15}$$

$$\mathrm{AF}(\hat{\mathbf{r}}) = \sum_{n=1}^{N} A_n e^{j\phi_n} e^{jk\mathbf{r}_n.\hat{\mathbf{r}}} \tag{2-16}$$

where $\mathrm{AF}(\hat{\mathbf{r}})$ is the array factor and

$$\mathrm{AF}(\hat{\mathbf{r}}) = \sum_{n=1}^{N} A_n e^{j\phi_n} e^{jk\mathbf{r}_n.\hat{\mathbf{r}}} \tag{2-16}$$

is the general representation of the array factor, which can be found by two methods. One is the element by element sum which is time consuming for larger arrays and the other is the infinite grating lobe sum. The infinite grating lobe sum is better for infinite arrays as it takes less time [2].

Using the element by element sum he array factor can be expressed as [2]

$$\mathrm{AF}(\hat{\mathbf{r}}) = A.N \frac{\sin(N(k_a - k_\phi)^{d_a}/_2)}{N sin(N(k_a - k_\phi)^{d_a}/_2)} e^{j\mathbf{r}_c.\hat{\mathbf{r}}} e^{j\phi_c} \tag{2-17}$$

where k_a is the product of the propagation constant and the cosine of the angle α between $\hat{k}$ and $\hat{a}$.

$$k_a = k cos\alpha \tag{2-18}$$

Array Factor as infinite grating lobe sum can be expressed as [2]

$$\mathrm{AF}(\hat{\mathbf{r}}) = e^{jk\hat{\mathbf{r}}.\mathbf{r}_c} e^{j\phi_c} \frac{1}{d_a} \sum_{p=-\infty}^{\infty} (-1)^{p(N-1)} \tilde{A}\left(k_a - k_\phi + p\frac{2\pi}{d_a}\right) \tag{2-19}$$

Where

$$\tilde{A}(k_a) = \int_{-\infty}^{\infty} A(a) e^{jk_a \boldsymbol{a}} da = \int_{-L/2}^{L/2} A(a) e^{jk_a \boldsymbol{a}} da \tag{2-20}$$

As the Fourier transform of the amplitude excitation is zero outside the interval

$-L/2 < \mathrm{a} < L/2$

2.2.6 Steering Main Beam and Grating Lobes

One of the advantages of the array antenna is that the main lobe can be steered up to different scan angles by changing the phase progression $\Delta\phi$ between the elements, using the beam-scanning feeding network of the array. We can write the relationship between the phase progression and the angle $\alpha = \alpha_0$ for which the array has the main lobe as,

$$\cos\alpha_0 = {}^{k_\phi}/_{k} = {}^{-\Delta\phi}/_{kd_a} \tag{2-21}$$

We can also express it in θ_0 of the spherical co-ordinate system by aligning the array along the $\hat{z}$ axis so that $\hat{a} = \hat{z}$,

$$\cos\theta_0 = {}^{k_\phi}/_{k} = {}^{-\Delta\phi}/_{kd_a} \tag{2-22}$$

When $\alpha_0 = 90°$, the $\Delta\phi = 0°$, we have a broadside array as it radiates normal to the array axis. For array to radiate along the axis, $\alpha_0 = 0°$ and phase difference becomes some value depending on lambda and element spacing $\Delta\phi = -kd_a = -\frac{2\pi d_a}{\lambda}$. We can also steer the main lobe to any direction in the φ plane [2]. Grating lobes also appear periodically nest to the main lobe according to

$$\left(k_a - k_\phi\right)d_a = -p2\pi, \qquad \text{for} \quad p = \pm1, \pm2 \ldots. \tag{2-23}$$

Grating lobes are undesirable and should be avoided in all cases unless they can be suppressed by element patterns. To avoid them the element spacing should be less than according to

$$d_a < \frac{\lambda}{1+|cos\alpha_0|+{}^{\lambda}/_{L}} \tag{2-24}$$

According to the above equation, the element spacing should be less 1λ for in a long broadside array and for end-fire array the element spacing should be less than ${}^{1}/_{2\lambda}$. The λ in the above equation should be used of the highest frequency of the bandwidth of the array.

2.2.7 Aperture Efficiency, Directivity and Affective Area

For aperture antennas and array, maximum directivity increases with electrically larger aperture of area A,

$$D_{max} = \frac{4\pi A}{\lambda^2} \tag{2-25}$$

In terms of aperture efficiency, which is the ratio of actual directivity of an aperture antenna due to imperfections to the maximum directivity given by equation $D_{max} = \frac{4\pi A}{\lambda^2}$ (2-25), we can write directivity as, [3]

$$D = \eta_{ap}\frac{4\pi A}{\lambda^2} \tag{2-26}$$

2.2.8 Electrical length of Antenna

Antennas electrical length can be different than its physical length. It is dependent on its physical length, the frequency and the dielectric constant. The electric length is expressed in terms of wavelength. For a half wavelength dipole resonating at frequency=150 MHz, the wavelength is equal to $\lambda = {}^{c}/_{f} = 2m$ the electrical length of the dipole equals to $l_e = 0.5\ \lambda$ and the physical length is $l_p = \frac{2}{2} = 1m$.

2.3 Modeling Techniques

Different modeling techniques were studied and implemented on the antenna model from the published papers that could help in designing of the array of self-grounded bowtie antenna to achieve the desired performance. The techniques which helped in achieving the results are mentioned below. However, the detailed implementation of these techniques on the antenna model is discuss in Section 3.2.

2.3.1 Inductive and Resistive Loading

Majority of the antennas work on the principal of resonance. An antenna will resonate at their resonant frequency when the capacitive and inductive reactances' cancel each other. At the resonant frequency antenna's impedance is purely resistive by definitions, which matches the characteristic impedance of the transmission line. At frequencies away from the resonant frequency the impedance can include some capacitive or inductance. An antenna which is shorter than its resonant length is electrical short antenna and has some capacitive reactance in its structure. Similarly, an antenna which is longer than its resonant length is electrical long antenna and has some inductive reactance in its structure.

We can change the electrical length of the antenna, by implementing capacitive and inductive loading. In this way we actually change its resonant frequency of the antenna [2]. In multiband antennas, we must use both inductive and capacitive loading to reach the multiple resonance frequencies. Different loading techniques have been implemented [5] on microstrip wide band antenna, which was used as reference in this work. In Capacitive loading slots are made in the planar structure that are perpendicular to the current direction. Where as in inductive loading slots are made parallel to the current direction. Both loading techniques were implemented on the antenna design.

2.4 Ultra-Wide Band Wireless Technology and Self-Grounded Bowtie Antenna

UWB is a radio wireless technology uses lower power consumption for high bandwidth communication. According to FCC, to be classified as UWB the bandwidth of the transmission needs to be more than 500 MHz [6]. UWB is spread over a wider range of the frequency spectrum and does not interfere with conventional narrow band communication. Because of its lower power consumption, it is well suited for short distance communication. It is also different from other conventional narrow band system transmission by means of transmission of information technology. UWB send short impulses over a broad spectrum.

2.4.1 UWB Advantages and Applications

UWB have low complexity and low cost due to their nature of transmission of signal. They do not require up-converters or down-converters [7]. Moreover, they can be incorporated in low powered circuits. They have noise like spectrums which are resistant to severe multipath and jamming [7] and this property makes them useful in military applications. The noise like nature of the UWB make unintended detection difficult, but it also causes no interference with other existing radio system. It can offer high data rates up to several hundred Mbps for communications links and it is believed that number of users in impulse radio communication is also large. Because of their good time domain resolution because of their narrow time domain-impulse nature. This means they can offer good timing precision which is beneficial in location and tracking applications. They are used a lot in short- radar applications such as surveillance operations, anti-crime and rescue operations. However, they do not offer deep material penetration along with time precision at the same time. UWB has gained popularity in MIMO networks as the combination of both can help achieve high data rates in communications, accommodate more number of users with less interference and efficiently utilize the spectrum.

2.4.2 UWB Antennas

UWB antennas are gaining a lot of importance in the wireless communication because of their faster data rates, low power consumptions and low cost. Especially in the areas where a large amount of data is needed to be transmitted over the radio frequency band 3.1-10.6 GHz for wireless communications [8]. Ultra-wide band antennas cover a wide frequency bandwidth (>500 MHZ), with multiband transmission of radio signals. One UWB antenna can replace many narrow band antennas which can reduce the number of antennas needed. This is beneficial in applications which require wireless device to operate in different frequencies. the radiation pattern of UWB antennas can be omni-directional and directional depending on the antenna design and applications.

UWB antennas can be classified into 4 categories [9]. The Bowtie dipoles, mono- and bi-conical dipoles and log-periodic dipoles array come under the category of scaled structures. These antennas have dipoles like characteristics with wider bandwidths and reasonable gain. They have a lot of applications in UHF terrestrial TV, HF communication for diplomatic traffic, electromagnetic compatibility measurements etc. However, they have bulky structures which

limit their applications [10]. The other category is the self-complementary structure which include many antennas such as the self-complementary spiral antennas. They are used in the commercially and military for many UWB applications like GPS. The equiangular spiral antenna have a low profile, circular polarization and omnidirectional [11]. Vivaldi antennas are also widely used for UWB applications and come under third category of travelling wave antennas. They have directional radiation patterns and have many uses in the field of medicines and radar and imaging system. However, they are of larger dimensions and bulky in nature, which is a problem where compact low-profile directional UWB antennas are required. Lastly, we have multiple-resonance structure as the last category of UWB antennas. They are low profile structures with omni-direction radiation patterns. The microstrip antenna in [12] generates multiple-mode resonance and surface plasma wave and has a very wide bandwidth of 3.3 GHz to 12 GHz. In [13] a multiple-mode slot-line radiator is proposed and developed which has a working band of 3.6 GHz -10.5 GHz. Many work has been done on UWB dielectric resonators, which is a new type of directional UWB antenna.

2.5 Self-Grounded Bowtie Antenna

The self-grounded bowtie antennas were first conceptionally realized in [9] and [14]. This paper also discusses the transition from bowtie to self-grounded bowtie antenna. It had three stimulated designs of the self-grounded bowtie antenna in CST microwave studio for a very wide bandwidth of 2-15 GHz and out of which one was manufactured, and the performance was analyzed. All the designs showed very promising stimulated results for the reflection co-efficient, radiation patterns and time-impulse response. The stimulated reflection-coefficient was almost less than -10dB and far-fields radiation patterns were stable and directive mostly, for the entire bandwidth. The manufactured designed of the self-grounded bowtie was very compact with promising results compared to other UWB antennas. The reflection co-efficient of the prototype was measured with a balun and it was less than -10 dB for most part of the bandwidth and less than -7 dB for the entire band. The measured radiation patterns were measured in $\varphi = 45°$ and were very directive for the entire band, with a directivity of 5.8 dBi for the entire band. The radiation efficiency was measured in the reverberation chamber, which was the measure of the ohmic losses and an important characteristic of the UWB antennas. It was almost 0 dB for the lower end of the band and increased for the higher frequencies. This prototype was very compact with good characteristics amongst the other UWB antennas. It had only one port and hence only linear polarization was possible. Moreover, since no optimization was done to this prototype, this design had a lot potential to be improved. There on many published papers have been written on self-grounded bowtie antennas.

In [15] a 4-port dual-polarized self-grounded bowtie antenna was presented. It was also a very wideband antenna with a bandwidth of 1.5-3 GHz. The directivity of each of the petal was 4.8 dBi. It was a very flexible compact antenna and it could be used as a 4-port antenna in the wireless communication in the MIMO system. It could also be used a directional 2-port dual polarized in line-of-sight applications such as radar and sensing systems. The antenna presented in [16] was also 4-port self-grounded antenna but it was only optimized for MIMO in the reverberation Chamber.

In [17] and [18] a linear array configuration is proposed of the improved version of the dual-polarized self-grounded bowtie antenna in [9] and [14] for Random Line-of-Sight Over-The-Air measurements. The proposed array in [17] has an 8×1 configuration and it is dual-polarized over the bandwidth 1.6-2.7 GHz. The measured reflection co-efficient of the manufactured prototype is below -10dB over the entire bandwidth. Moreover, the realized gain for both the polarization is 13-18dB. The dimension of each array element is $110\ mm\ by\ 110\ mm$. Which correspond to λ at the highest frequency of the bandwidth. It was this design of the self-grounded bowtie antenna that was used for modelling and optimization in the project. The self-grounded Bowtie can be also applied to medical applications [19] and [20].

3 SINGLE ELEMENT DESIGN AND SIMULATION

This chapter covers the specifications of the antenna, and the design and simulation of the single element of the array antenna. The self-grounded bowtie antennas in the published papers discussed above showed good performance for an ultra-wide-band antenna amongst other UWB antennas. A phased array configuration of 4×4 of the self-grounded bowtie antenna was designed for a different bandwidth than the published papers.

In the previous research papers [17] and [18], a linear array of N×1 was designed and a prototype was manufactured. In this project, for the first time a N×N phased array antenna of the self-grounded bowtie has been designed and optimized. The antenna in [17] was used for modelling and optimization in the project to achieve the desired specifications and results discussed below.

Such array antenna is also intended to be manufactured as a single prototype. However, due to time constraints the manufactured prototype's results were not covered in this report.

3.1 Designs Specifications

The aim of the project was to design and analyze a dual polarized phased array of self-grounded bowtie antenna in both planes, E- and H-plane. The main aim was to achieve a directional scanning of the array up to $\pm 60°$, with good impedance matching and directivity. However, this was not a deemed requirement and beam scanning up to $\pm\,45°$ was considered good enough. Since this antenna is dual-polarized, good isolation between the polarizations was an important goal. Along with that, good isolation between the elements of the array was also an important aspect of the array antenna. The single element had to be compact. An important goal was to achieve the required bandwidth of 3.1-4.8 GHz with a good reflection co-efficient of -15 dB for the single element and -10dB for the array. This project was conducted with the aim to manufacture a prototype, therefore the antenna had to be modelled in such a way that the manufacturing could be done faster and cheaper without compromising the results.

3.1.1 Bandwidth

The bandwidth of interest for this prototype was 3-5 GHz, which later got changed into 3.1 GHz- 4.8GHz for the array antenna.

3.1.2 Element Spacing and Beam Scanning of the array antenna

To scan the main beam of the array, the element spacing of the elements in the array antenna needs to fulfill the criteria to avoid grating lobes for the corresponding scan angle α_0. When the array is scanning up to $\pm\,60°$,the main beam is at $60°$ from the broadside, and therefore $\alpha_0 = 30°$.

We can calculate the element spacing, d_a to avoid grating lobes:

$$d_a < \frac{\lambda}{1 + |cos\alpha_0| + {}^{\lambda}/_{L}}$$

$$d_a < \frac{{}^{c}/_{f}}{1 + |cos\alpha_0|}$$

$$d_a < \frac{{}^{3.10^8}/_{4.8.10^9}}{1 + |\cos 30|}$$

$$d_a < 33.49\ mm$$

The term ${}^{\lambda}/_{L}$ was ignored in the calculations as it becomes very small for a large value of L, which is the length of the array. Moreover, d_a was calculated at the highest frequency of the bandwidth which is $f = 4.8\ GHz$.

3.1.3 Number of ports and Polarizations

The symmetrical 4 ports geometry was maintained with good isolation between the ports. The array antenna should be excited for single and dual polarization. Therefore, isolation between the two polarizations was an important feature and needed to be very high for the array design. This was analyzed for different scanning angles as well in a 2-port network of the whole array with its embedded S-parameters.

3.1.4 Elements Isolation

To achieve good isolation between each array element, boundary walls around all sides of the element were added with the wall height of ${}^{\lambda_0}/_{4}$ in the element [17], which was later resized for optimum performance of the antenna in the array.

3.1.5 Polarization Isolation

The single element was optimized for reflection co-efficient less than -15 dB over the entire bandwidth, when the opposite ports were excited with differential excitation. Moreover, the original self-grounded bowtie antenna in [17] had a good intrinsic isolation between the differential excited pairs of ports, which also helped to achieve good isolation between the two polarizations.

3.1.6 Directivity

Directional radiation patterns with good directivity were required to steer the beam.

3.1.7 Easy Manufacturing

Many modifications were made to make manufacturing and assembling process easy, fast and cheap without compromising the antenna performance. It was important that the total height of the self-grounded bowtie element was less than *40 mm*. Secondly, the petals were folded, so

they had a curved curvature/surface rather than flat top. Because the element was so small and compact, the folded petals made the assembling process easier and more practical than flat petals' top. The diameter of the coax cable connections in the elements were modified so that they are exactly like the available ones in the market. Moreover, for the antenna to be 'assembly friendly', it was established that the minimum gaps between the different parts of the element were at least *1mm* apart. Otherwise, other means had be taken to ensure that they do not get in contact with each other. For example, to prevent the corner of one petal of the antenna to be in contact with other petal, plastic could be made stand in between them but, in that case, too it would affect the performance anyway.

3.2 Element Modelling and Design

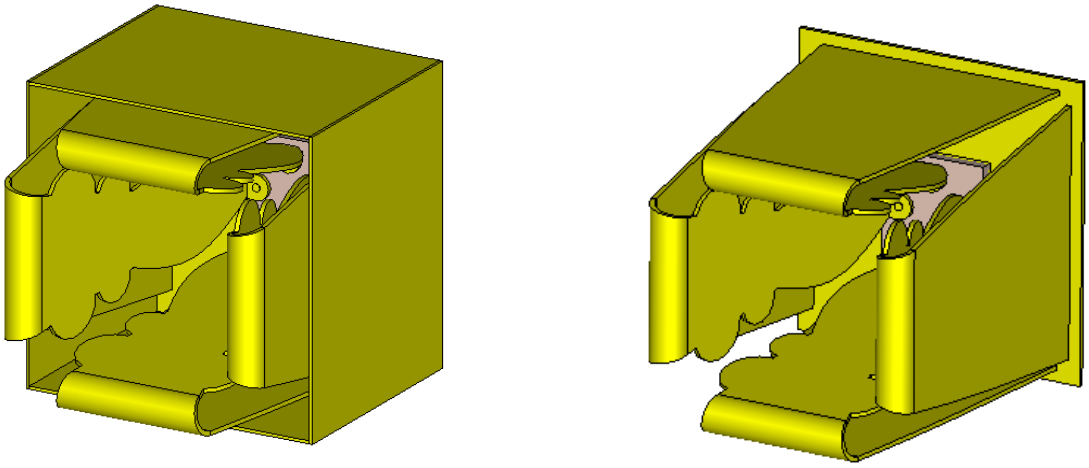

(a) (b)

Figure 3.1 Single Element Design (a) with boundary walls, (b) without boundary walls

The single element was designed for an array configuration. It needed to meet all the specifications discussed above. The modelling and optimization of the single element was done with periodic boundary conditions for x- and y-axis. The reflection co-efficient, far-field patterns and gain were mainly monitored. Unit cell boundary conditions were used for scanning of the main beam and reflection co-efficient, far-field patterns and directivity were monitored. The single element was optimized for a minimum reflection co-efficient of -15 dB over the required bandwidth with good isolation between the element pair of differential ports.

3.2.1 Element Dimensions

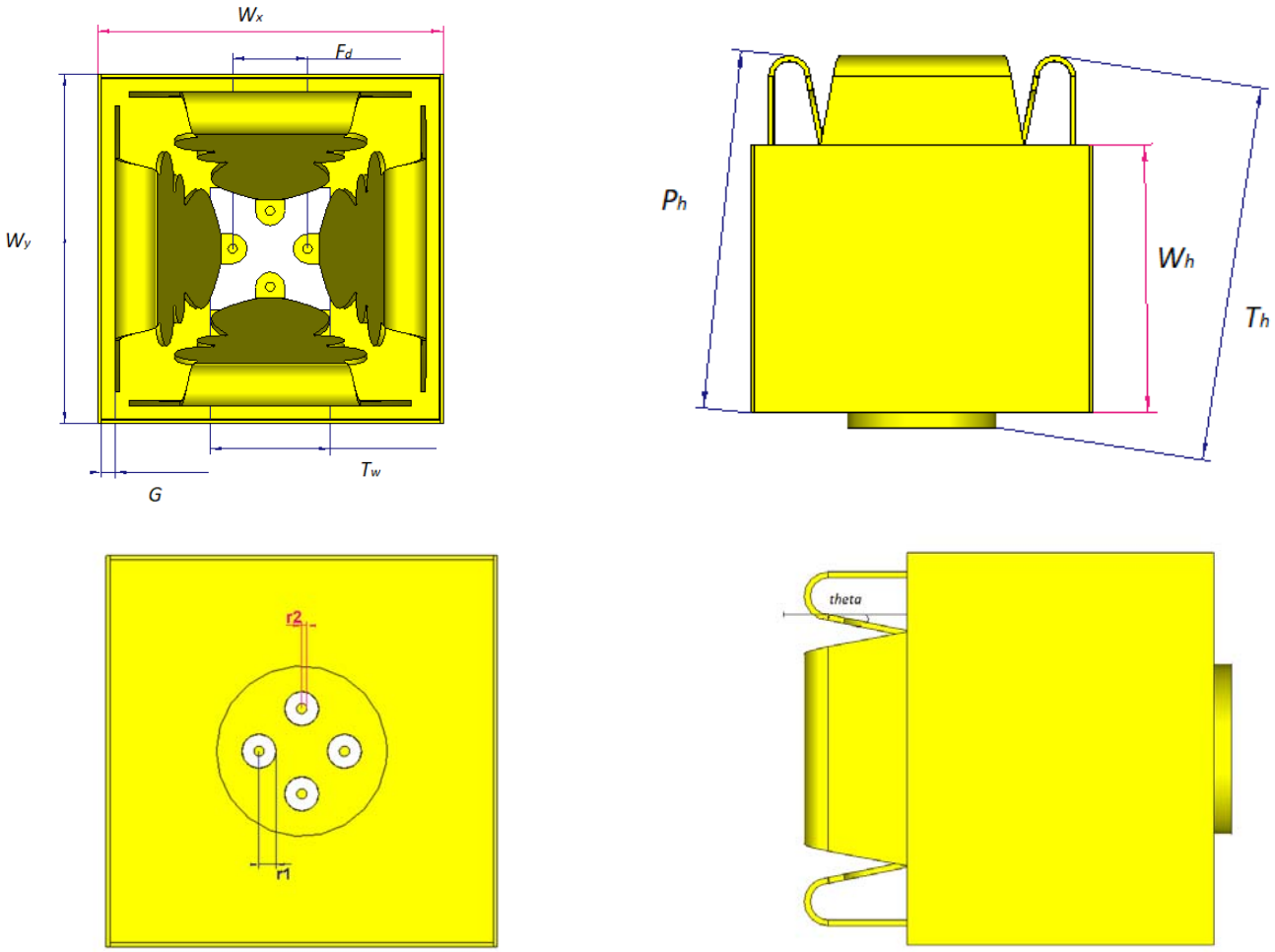

Figure 3.2 Element Geometry and Dimensions

A compact element was designed for the array. Therefore, strict modelling was performed to meet the criteria set by the design specifications for the dimensions of the element. The most important being the element spacing, the height of the element and minimum gaps between the different parts of the antenna.Table 3-1 shows the different dimensions of the single antenna element.

Parameters/ mm										
W_y	W_x	$theta$ $\theta°$	P_h	W_h	T_w	F_d	T_h	G	r_1	r_2
34.08	34.08	78.5	37.15	26.90	11.92	7.45	39.68	1.34	1.49	0.46

Table 3-1 Dimensions of the Element

3.2.2 Element Spacing

The antenna in [17] was symmetrical in its design and shape . It was rescaled to a smaller antenna to achieve the condition for element spacing. An element spacing of $d_a = 34.08\,mm$ was achieved after the final optimization that met single element design specifications.

When the element in [17] was rescale to the smaller antenna, the bandwidth shifted to higher frequencies. To shift the bandwidth to the required frequency, range many modifications have been implemented in the design. To begin with the element parameters were analyzed by performing different parameter sweep to see their effect on the bandwidth of the antenna element.

3.2.3 Height of the Element

The antenna became an electrically short antenna when it was rescaled to a small size and had some capacitive reactance in its structure. For this purpose, the largest dimension of the antenna apart from its length or width (element size) was increased so that the element spacing was not affected.

The largest dimension of the antenna was the total length of the petal when it was flat. Parametric sweep of different parameters controlling the height of the petals were performed. It was observed that when the height of the petals was increased, the bandwidth shifted to lower frequencies. This could be mainly because as the height is increased, the return currents have longer paths to travel. Although this modification shifted the bandwidth to lower frequencies, it degraded the reflection coefficient.

3.2.4 Shape of the Petals of the Element

The self-grounded bowtie antenna had four symmetrical petals. The petals were positioned in such a way that two petals faced the other two. They extended from the ground plane, were bended almost half way through their lengths and joined in the center of the antenna at the feeding point.

Inductive loading was applied on the petals of the antenna. By observing the direction of the surface currents, vertical and horizontal slots were made in different places of the petals. Semi-circular slots were cut out from the edges of the petal near the feeding. But it rather shifted the bandwidth to the higher frequencies. Therefore, instead of cutting slots from the edge two circles were added to the petals along the both sides, which helped to achieve the required bandwidth. Moreover, after the final optimization, the minimum gap between petals was of $0.80\,mm$. As this gap was reduced and the petals came closer, the performance was improved. This might have caused reduced capacitance in the structure. Thus, the addition of the circles in the petals might had acted as inductive loading. It could also have had the same effect due to longer petal's lengths as the circles 'circumference was added to the overall lengths of the petals.

Again, different parameters controlling the shape and the lengths of the petals were swept in the parameter sweep to see the effect on the bandwidth as well as on the reflection co-efficient. These parameters were then optimized in the final optimization of the antenna to improve the reflection co-efficient.

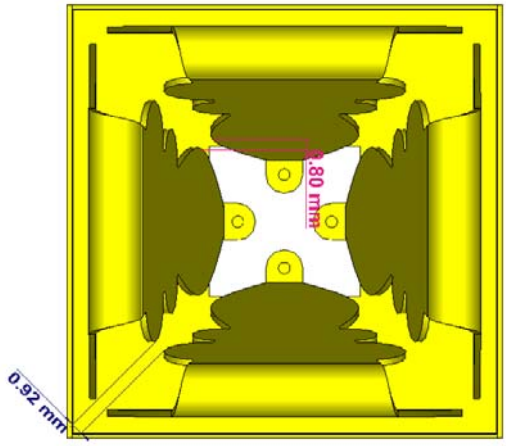

Figure 3.3 Single element structure showing the minimum gap between the petals

3.2.5 Boundary Walls of the Single Element

Initially the boundary walls were added to maintain isolation between the elements in the array, but later it was observed from surface current plots of the antenna that the walls also had high surface current at the top and bottom parts and contributed to the resonance in the bandwidth.

In the final element design, after the final optimization, the height of the walls was $W_h = 26.90\,mm$, which was lower than the height of the petals,$P_h = 37.mm$. When W_h was increased to bring it level with petals' height, the resonance at the high frequency of the bandwidth was shifted towards the higher frequencies and the low frequency resonance was diminished. Therefore, it was kept as $W_h = 26.90\,mm$ as it gave the desired results. It could be due to mutual coupling between the array elements, since lowering the walls' height could result in coupling between the array elements.

It could be that the mutual coupling between the petals and the walls as the gap between them is very small of $1.34\,mm$ helped in shifting the bandwidth. It could also be due to mutual coupling between the array elements, since lowering the walls' height could result in coupling between the array elements.

Inductive and resistive loading were implemented on the walls to have resonances in the desired frequency band. Rectangular slots were added in different areas of the walls. It was observed that these slots had no effect on the reflection co-efficient when they were in the middle of the walls, as the surface currents are minimum in the middle of the walls. But in the bottom and the top part of the walls, where the surface currents were the highest, when slots are added, the lower frequency resonance diminished as the slots got bigger in the top and bottom of the walls.

3.2.6 Feeding and Ports of the Element

Two more parameters which had a strong influence on the bandwidth were the distance between the ports in the feeding (feeding distance) and the size of the ports. Both parameters changed port impedances. The distance between the ports was optimized to achieve the desired bandwidth with good reflection co-efficient. It was observed that when feeding distance was increased, reflection co-efficient degraded and bandwidth became narrower. Larger feeding distance also increased the distance between the petals. Better reflection co-efficient and wider bandwidth was achieved after final optimization, when slightly bigger diameters of the ports of the coax cable in the antenna structure were selected with line impedance of 50 ohms.

3.2.7 Ground Plane of the Element

The petals must be in contact with the ground plane. Poor or partial contact with the ground plane degraded the reflection co-efficient and shifted the bandwidth.

3.3 Single Element Simulation Results

The simulations were performed in CST-Computer Simulation Technique. The single element was designed for an array configuration. The modelling and optimization of the single element were done in periodic boundary conditions for the axis-x and -y in TDS, Time Domain Solver, because it was faster than FDS, frequency domain solver. For beam scanning, unit cell boundary conditions were used in FDS.

3.3.1 Single Element Broadside Radiation

After the final optimization of the element, a bandwidth of 3.2GHz- 4.9GHz was achieved with a reflection co-efficient less than -15dB over the entire bandwidth for broadside radiation, as it is shown in Figure 3.4 (a) Reflection co-efficient when we simultaneously excite the opposite ports
with differential excitation of single element in periodic boundary conditions(a). This was when we simultaneously excite the opposite ports with differential excitation and because of the symmetrical nature of the antenna, opposite ports had same reflection co-efficient for this excitation. Isolation between the two polarizations was checked with a simple feeding network of ideal power dividers and phase shifters, in CST schematics. Which basically uses antenna's embedded S-parameters to perform different circuitry calculations. The isolation between the polarization was less than $-115\ dBi$ over the entire bandwidth as shown in the Figure 3.4 (b).

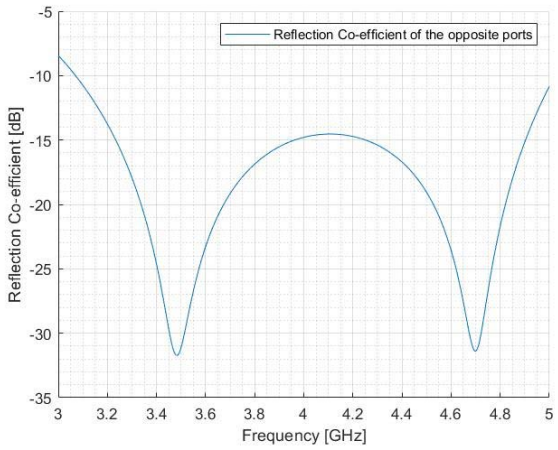

(a)

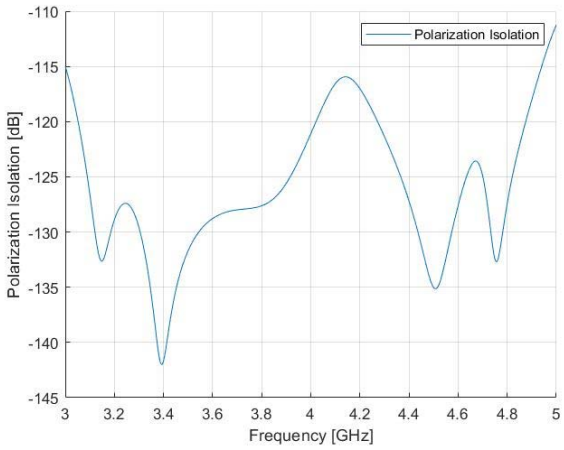

(b)

Figure 3.4 (a) Reflection co-efficient when we simultaneously excite the opposite ports
with differential excitation of single element in periodic boundary conditions (b) Isolation between the polarizations for differential excitation of the ports of the single elements

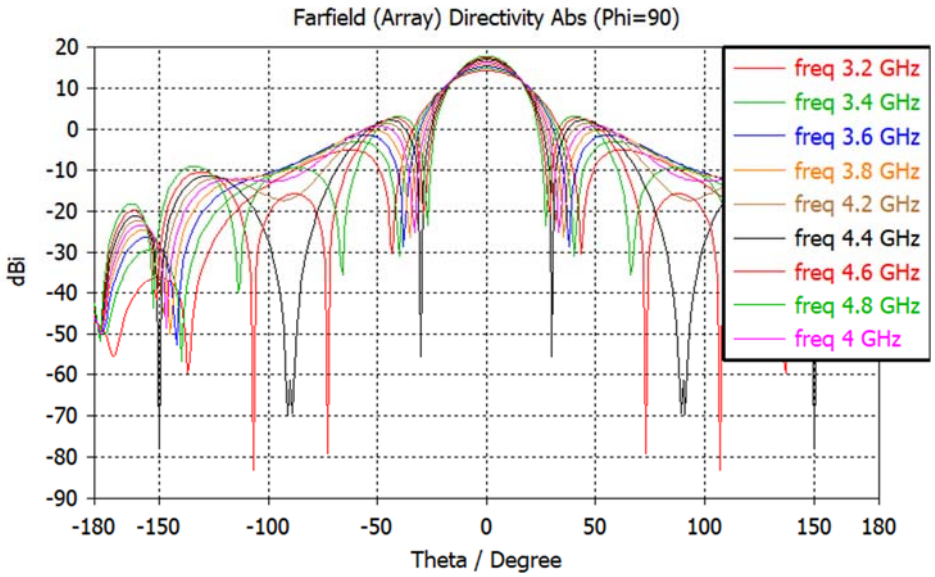

Figure 3.5 Far-field Cartesian plot for broadside radiation
of the single element.

Figure 3.5 shows the far field Cartesian plots of the single element in the broadside direction for frequencies 3.2-4.8 GHz. In the broadside direction, the side lob levels were less than the main lobe by 14.7 dB and grating lobes were visible in the entire bandwidth. In broadside radiation, a directivity of 14.3-17.8 dBi was achieved over the bandwidth 3.2-4.8 GHz as shown in the Figure 3.5. The gain and directivity of the antenna were same as the antenna had a radiation efficiency of 100%.

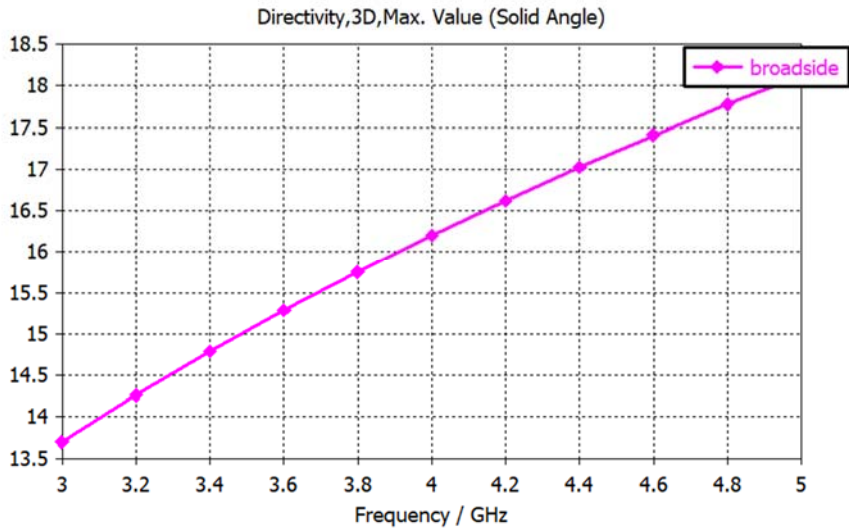

Figure 3.6 Single element directivity plot for an array (4× 4) for broadside radiation.

3.3.2 Single Element Main Beam Scanning up to $\pm 30°$, $\pm 45°$ and $\pm 60°$ in E- and H-planes.

Main beam scanning was done in FDS with unit cell boundary conditions in CST. Theta was scanned for broadside, $\pm 30°$, $\pm 45°$ and $\pm 60°$ in E- and H-planes. Since the antenna had dual polarizations which were orthogonal to each other. So, H-plane in one polarization corresponded to E-plane in the other polarization.

For the far-field plots, I used the embedded element pattern and the array factor to calculate the total radiation pattern in CST. This was done for an array of 4 x 4 for different scanning angles up to $\pm 60°$ to check for grating lobes and directivity. The directivity plots over frequency were also calculated for an array of 4 x 4 in post-processing.

3.3.2.1 Reflection Co-efficient, Gain, Directivity and grating lobes of the Single Element

In for scanning up to $\pm 30°$ in the E-plane, reflection co-efficient better than -10 dB was achieved over the entire bandwidth of 3.2-4.9 GHz as shown in the Figure 3.7 (a). For scanning up to $\pm 45°$, the reflection co-efficient was less than *-10 dB* for bandwidths (3.2-3.6 GHz and 4.6-4.7 GHz). However, while scanning up to 60° no part of the bandwidth less than -10 dB.

In H-plane, for scanning up to $\pm 30°$,the reflection co-efficient of less than $-10\ dB$ for two frequency bands: 3.2-3.75GHz and 4-4.9 GHz. These multi-bands get narrow by roughly 700 MHz on both sides as the degree of scanning was increased (for ±45°: 3.27-3.7 and 4.10- 4.9 GHz, for ±60°: 3.34-3.64 GHz and 4.29-4.65 GHz). We could also see a resonance in the reflection co-efficient plot in H-plane only in Figure 3.7(b). That could we due to blindness caused by the surface wave in case of an infinite array. However, it disappeared in the array simulations. It could also be due to some simulation error.

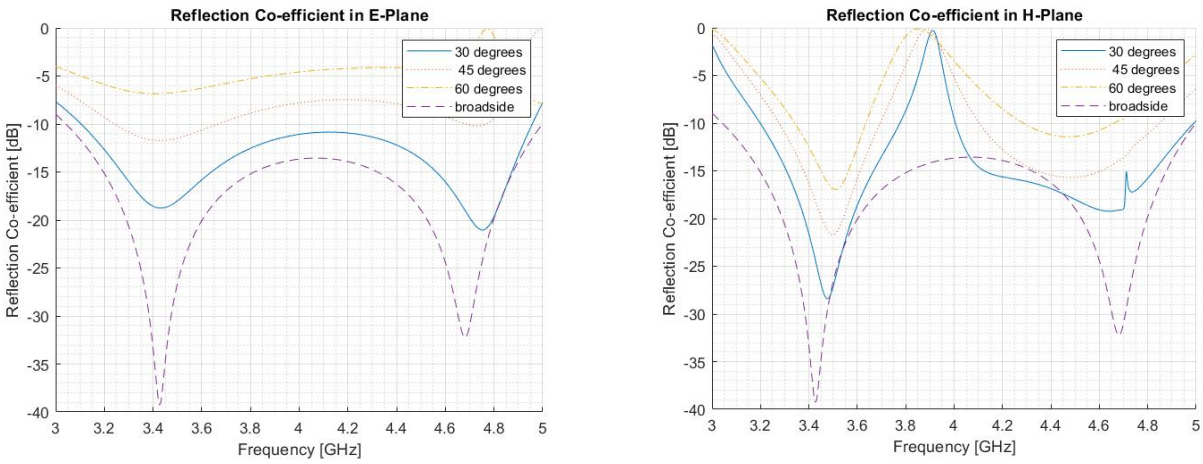

(a) (b)

Figure 3.7 Reflection Coefficient for different scanning of the single element in(a) E- and (b) H-plane.

For the element, directivity for an array of 4×4 for the broadside direction and scanning were plotted over frequency. The directivity range over the bandwidth for scanning up to ±30°, ±45°, and ±60° were 13.1-17.6 dBi, 12.5-16.7 dBi and 11.8-15.6 dBi respectively as shown in the

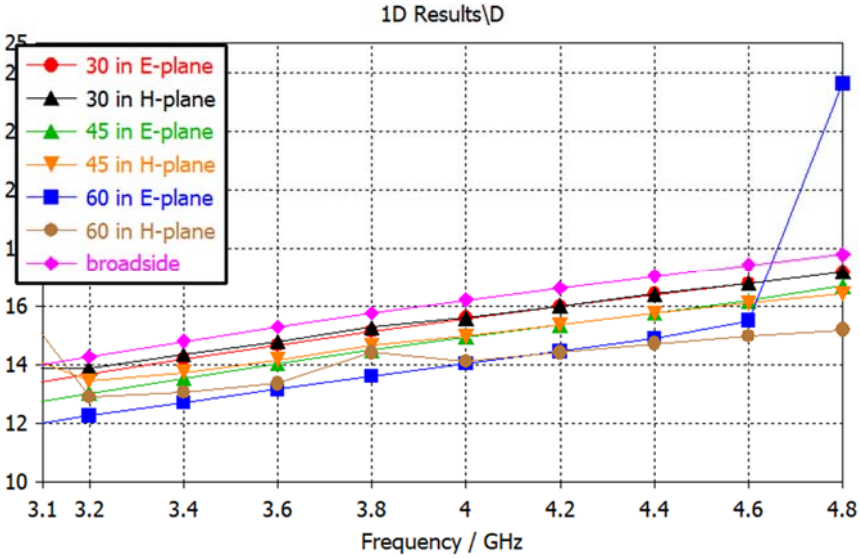

Figure 3.8. Grating lobes do not start appearing until scanning for ±60° for frequencies higher than 4.4 GHz.

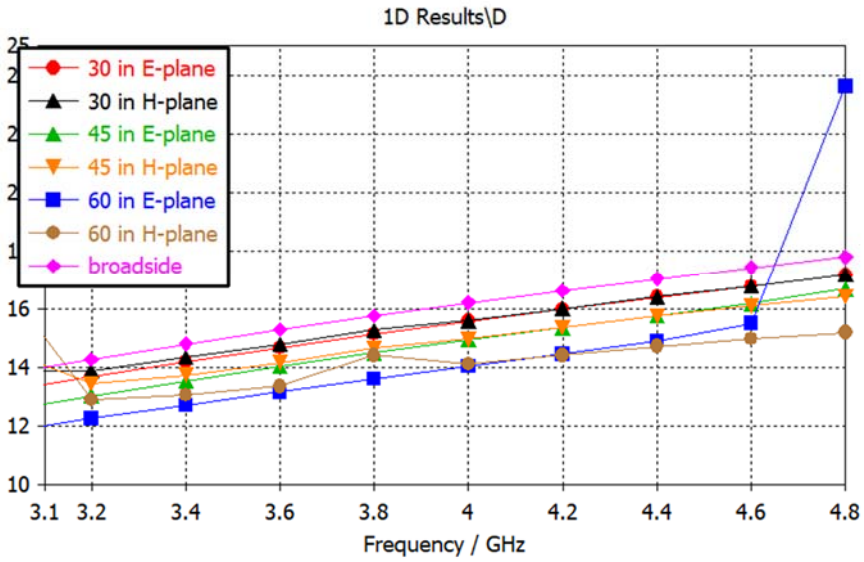

Figure 3.8 Directivity plot for an array (4× 4) for broadside direction and scanning up to ±30°, ±45° and ±60° in E- and H-plane.

3.3.2.2 Far-Field Plots of the Single Elements in infinite periodic boundary condition in E- and H-plane:

E-Plane

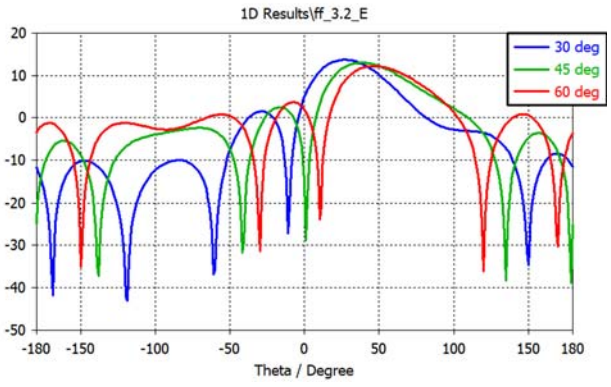

(a)

H-Plane

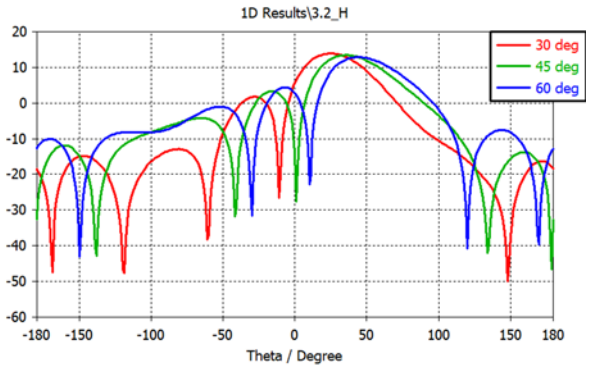

(b)

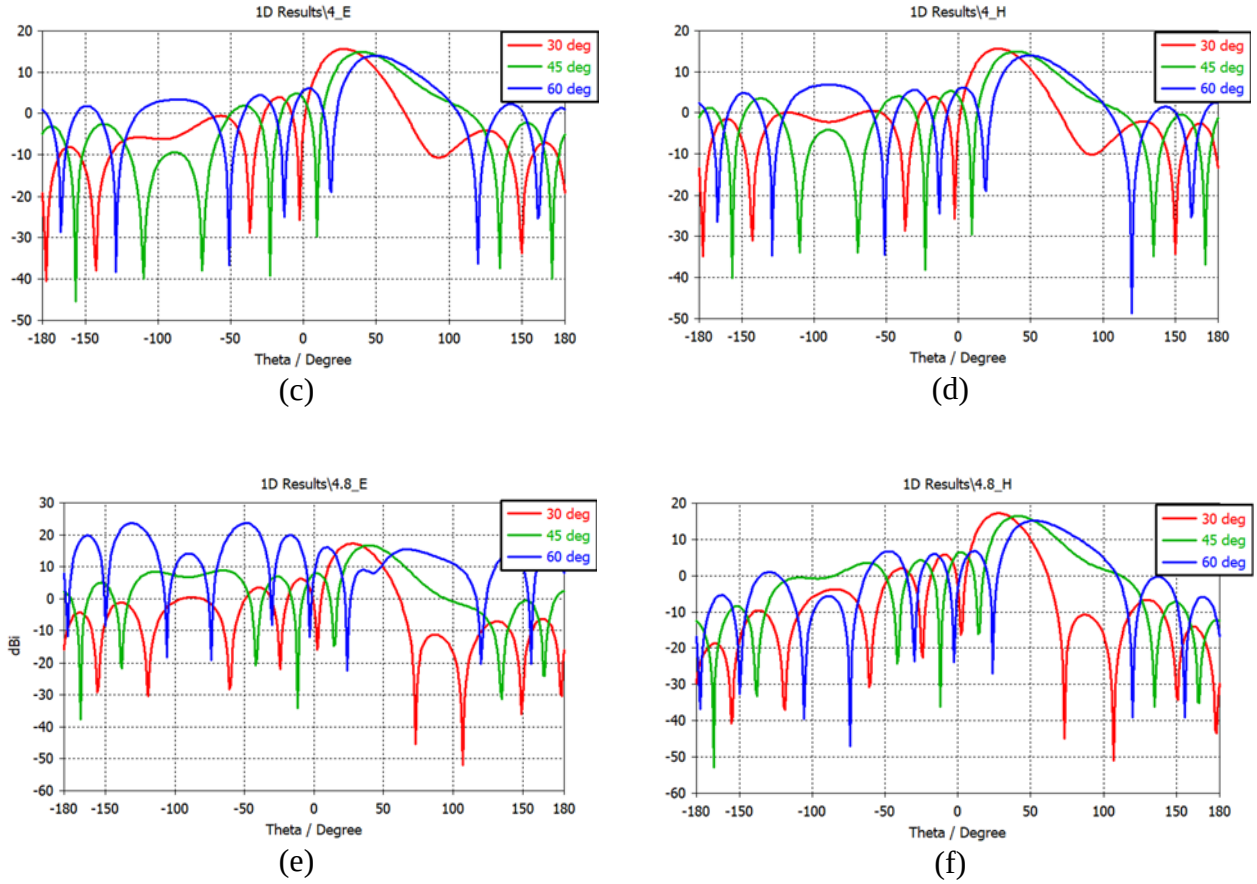

Figure 3.9 Far-field plots of the single element in infinite periodic boundary condition for different scanning's for frequencies (a) & (b) 3.2 GHz, (c) & (d) 4 GHz and (e) & (f) 4.8 GHz in E- and H-planes respectively.

4 ARRAY DESIGN AND SIMULATION RESULTS

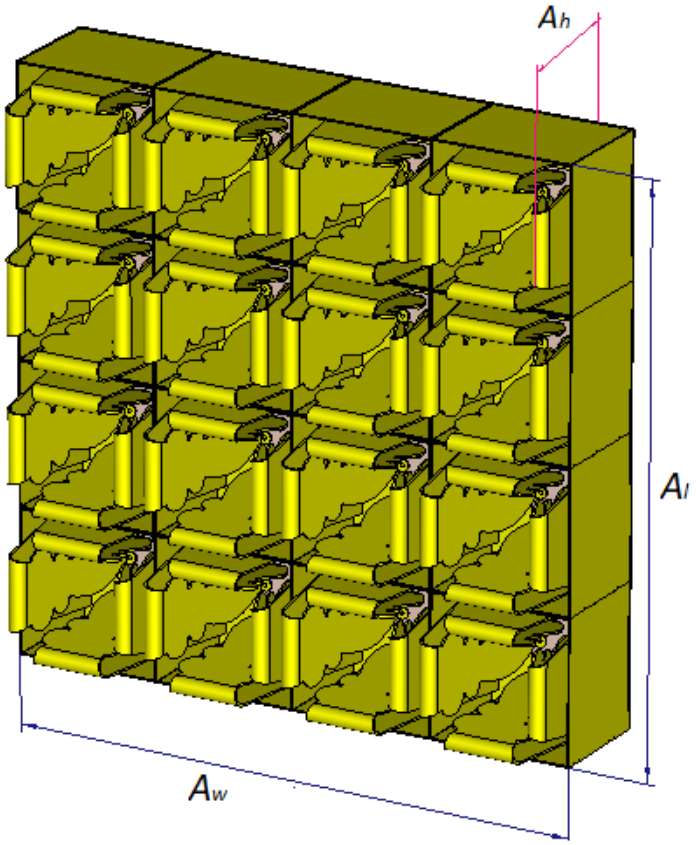

Figure 4.1 Front view the array design in CST

This chapter covers the array simulation and all the different results that were computed to analyze the performance of the array antenna. The single element was designed in a way so the final array would automatically meet the goals and therefore no optimization for the array was needed.

Parameters/mm		
A_w	A_l	A_h
136.70	137.70	39.68

Table 4-1 Dimensions of the array

Array simulations were done with 'open boundary conditions' in TDS. Many different results were computed for the array antenna design. Reflection co-efficient of all the individual ports stimulated for simultaneous excitation for the two polarizations were obtained. To see the combined-reflection co-efficient of each pair of ports for each polarization, waveguide ports in

the antenna structure were replaced by discrete ports. This was not done with all elements. This point is further explained in the coming sections of the report.

Moreover, S-parameters of a 2-port network of the whole array was calculated in CST, Schematics, from embedded S-parameters of the antenna. This is further discussed in the section 4.1.5

4.1.1 Broadside Radiation of the Array:

25 26 28 27 Element 13	53 54 56 55 Element 14	57 58 60 59 Element 15	61 62 64 63 Element 16
21 22 24 23 Element 9	41 42 44 43 Element 10	45 46 48 47 Element 11	49 50 52 51 Element 12
17 18 20 19 Element 5	29 30 32 31 Element 6	33 34 36 35 Element 7	37 38 40 39 Element 8
1 2 4 3 Element 1	5 6 8 7 Element 2	9 10 12 11 Element 3	13 14 16 15 Element 4

Table 4-2 Front view of the 4x4 array showing symmetry for reflection co-efficient for broad scanning for one polarization.

When the array was simulated for broadside scanning, even numbered ports (shown in the Table 4-2) were excited for horizontal polarization and odd numbered ports were excited for the vertical polarization. However, the array had same results for both polarizations. Therefore, the report contains results for only one polarization, and subsequent chapters contains results for horizontal polarization.

Because of the symmetrical nature of the array, ports of same colors had same reflection co-efficient. Meaning, ports 2, 14, 26 and 62 (shown in the Table 4-2) had same reflection co-efficient as for horizontal polarization and similarly ports 1, 13, 25 (shown in the Table 4-2) and 61 had same reflection co-efficient for vertical polarization. This trend was symmetrical with respect to the middle bold vertical and horizontal lines of the Table 4-2. For easy understanding, antennas in the same colored boxes had same reflection co-efficient for their ports corresponding to when excited for vertical and horizontal polarization. This trend was seen for broadside and for other scanning's as well.

4.1.2 Directivity, Grating lobes and Side-lobe Levels of the Array in Broadside Direction

In the broadside direction the array antenna has a directivity range of 14.2- 17.3 dBi over the bandwidth of 3.2-4.8 GHz. No grating lobes appear in the broadside far-field radiation pattern radiation shown in Section 4.2.8 and 4.2.15. The side-lobes are less than the main beam by 16.8 - 13.8 dB.

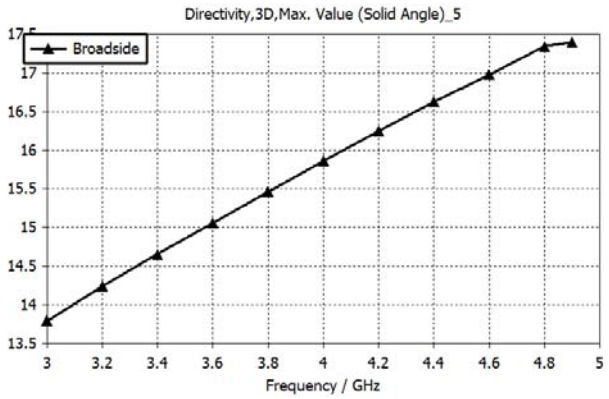

Figure 4.2 Directivity plot of the array in broadside direction.

4.1.3 Individual Port Reflection Co-efficient of Elements in the Array in Broadside Direction

Almost all ports of the array had reflection co-efficient less than -10 dB for the entire bandwidth. Ports having reflection co-efficient similar to ports 4 and 20 only had them for slightly narrow bandwidths. This was because antennas of these ports were on the boundary of the array and had more losses. Port 4 had reflection co-efficient less than -10 dB for 3.2-3.7 GHz and 4.6-4.9 GHz. Port 20 had reflection co-efficient less than -8 dB for entire bandwidth.

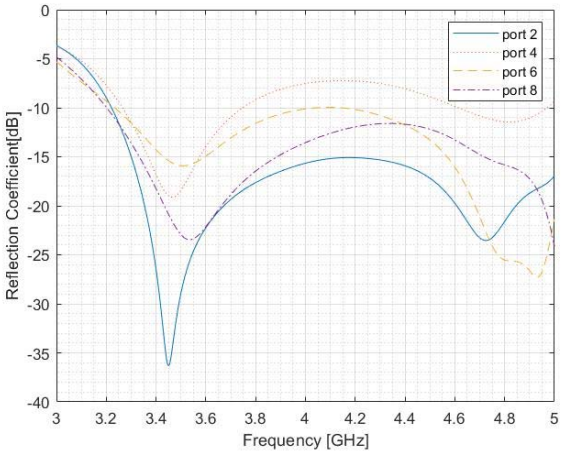

Figure 4.3 Reflection co-efficient of ports 2, 4,6 and 8 in the array for broadside direction

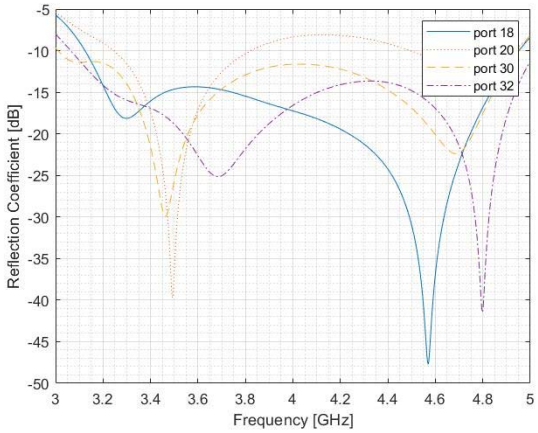

Figure 4.4 Reflection co-efficient of ports in the array 18,20,30 and 32 for broadside direction

4.1.4 Combined Reflection Co-efficient of Individual Elements in the Array in Broadside Direction

To have combined reflection co-efficient of the pair of ports of each element, we replaced individual waveguide ports with a discrete port. We did this for elements 1, 2, 5 and 6 only, which are shown in the Table 4-2 Front view of the 4x4 array showing symmetry for reflection co-efficient for broad scanning for one polarization.. Generally, it was seen close to the average of the individual reflection co-efficient of the ports. Combined reflection co-efficient was analyzed to see how much the input reflection co-efficient the power amplifiers of the feeding network would be getting from each element of the array.

All elements of the array had reflection co-efficient less than -8dB for the entire bandwidth shown in Figure 4.5. The inner most elements (6,7,10 and 11) have reflection co-efficient than -10 dB for the entire bandwidth. The corner elements (1, 4 3 and 16) had reflection co-efficient of less than -10 dB for 3.3-4.8 GHz. Element 2, 3, 14 and 15 had reflection co-efficient of less than -10 dB for 3-4.6 GHz. Element 5 had a reflection co-efficient of less than -10 dB for 3.3-5 GHz.

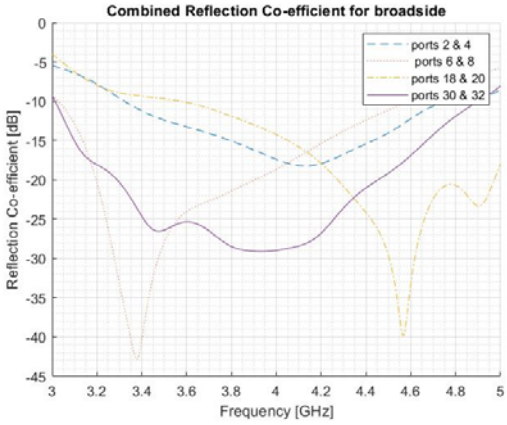

Figure 4.5 Combined reflection co-efficient of the ports for elements 1, 2, 5 and 6 for broadside direction.

4.1.5 2-Port Network of the Array Antenna

A 2-port network of the array antenna was made in the CST Schematics with a simple feeding network of only consisting of ideal power divider and ideal phase shifter. Each port was attached to one of the dual polarization of antenna. In this way, we could calculate total reflection co-efficient of each port and the isolation between each polarization from the imbedded S-parameters of the array.

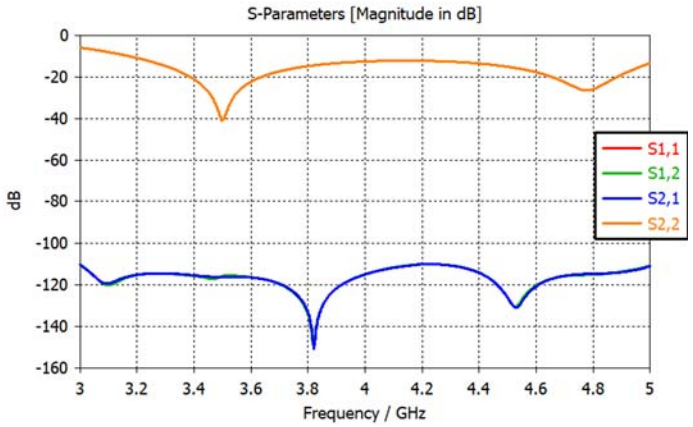

Figure 4.6 2-port S-parameters for broadside scanning for the array antenna

S11 and S22 in Figure 4.6 are the reflection co-efficient for each polarization, which was less than -15 dB for the entire bandwidth 3.2GHz-4.9 GHz. S21 and S12 are the isolation between each polarization and it was less than -110 dB for the entire bandwidth.

4.2 Array Main Beam Scanning up to $\pm 30°$, $\pm 45°$ and $\pm 60°$ in E- and H-planes for One Polarization

Phase differences $\Delta\phi$ were calculated according to equation $\cos\theta 0 = {k_\phi}/{k} = {-\Delta\phi}/{kd_a}$ (2-22) for the scanning angles at the central frequency 4GHz. It was assumed that the software CST calculates the phase difference at the rest of frequencies itself. This assumption was made because in solver (TDS), while entering the phase shifts for each port, it asked for the reference frequency for the entered phase shift values.

The elements of the array were excited for horizontal polarization in E-plan and then H-plane. To excite the array, the opposite ports of all the elements were simultaneously excited with differential excitation for in E-plane and then H-plane. The antenna had dual polarizations which were orthogonal to each other. So, H-plane in one polarization corresponded to E-plane in the other polarization. By, simulating the array for one polarization in the E- and H-plane we analyzed the array completely and simulation for the other polarization was not required.

Theta $\theta°$	Phase difference $\Delta\phi$
$30°$	$-82.0080°$
$45°$	$-115.9768°$
$60°$	$-142.0420°$

Table 4-3 Phase difference $\Delta\phi$ for different beam scanning

4.2.1 Directivity, Grating lobes and Side-lobe Levels of the Array for Main Beam Scanning in E- and H-planes

The directivity range over the bandwidth for scanning up to $\pm 30°$, $\pm 45°$, and $\pm 60°$ were 13.2-16.8 dBi, 13.6-15.7 dBi and 12.7-13.7 dBi respectively as shown in the Figure 4.7. In the far-field radiation patterns, the sidelobe levels were less than the main beam magnitude by 10.5 dB and 7.5 dB for scanning up to ±30° and ±45° respectively in both the planes and grating lobe do not appear while scanning up to ±45° in both planes. Grating lobes only start appearing for frequencies higher than 4.2 GHz while scanning up to ± 60 degrees and for frequencies lower than that, the sidelobe levels were less than the main beam magnitude by 7.6 dB.

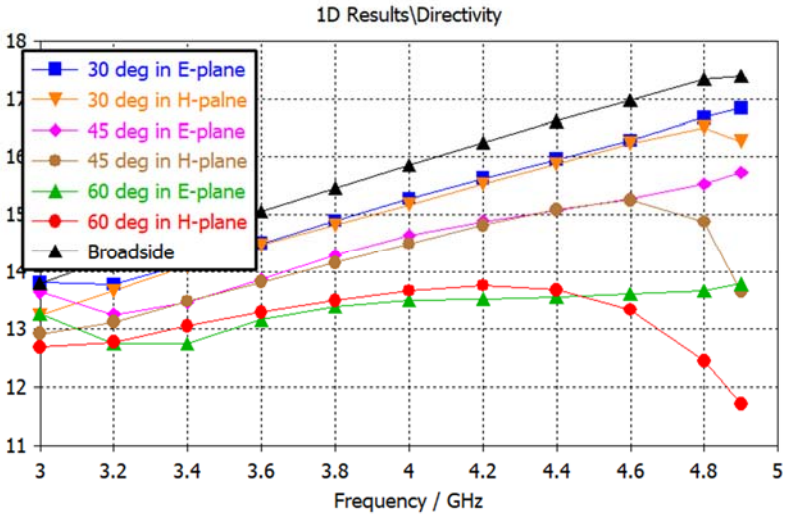

Figure 4.7 Directivity plot of the array for broadside direction
and main beam scanning up to ±30°, ±45° and ±60° in E- and H-planes

4.2.2 Individual Port Reflection Co-efficient of Elements in Array for Scanning up to ±30° in E-plane

All ports for the array had reflection co-efficient less than -6 dB for the entire bandwidth. For reflection co-efficient less than -10 dB, the bandwidth became narrow for individual ports. For elements on the boundary of the array (same colored boxed elements as: 1, 2 and 5), had bandwidth of 3.1-3.7 GHz for which the reflection co-efficient was less than -10 dB. Which was quite decent for elements that were on the boundary of the array. They are prone to more losses. Elements in the middle of the array (elements: 6, 7 10 and 11), had two bands for which their reflection co-efficient were less than -10 dB from 3-3.6 GHz and 3.2-3.6 GHz.

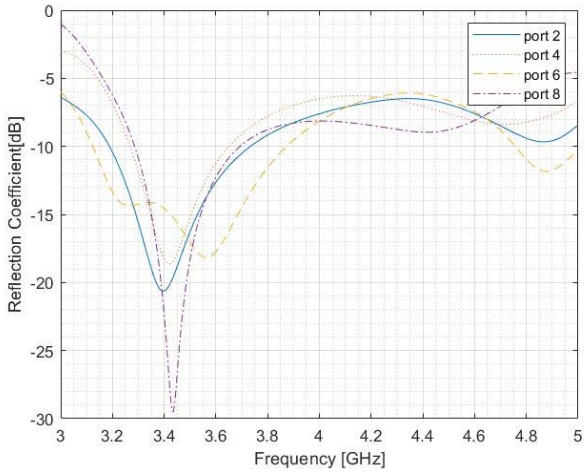

Figure 4.8 Reflection co-efficient of ports 2, 4,6 and 8 in the array
for scanning up to ±30° in E-plane

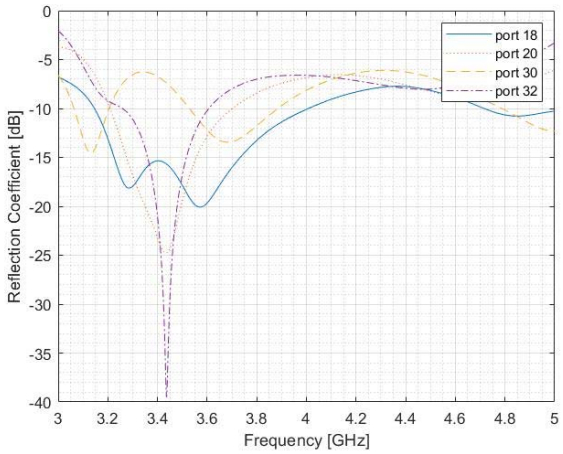

Figure 4.9 Reflection co-efficient of ports 18,20,30 and 32 in the array for scanning up to ±30° in E-plane

4.2.3 Combined Reflection Co-efficient of Individual Elements in Array for Scanning up to ±30° in E-plane

To have combined reflection co-efficient of the pair of ports of each element, we replaced individual waveguide ports with a discrete port. We did this for elements 1, 2, 5 and 6 only, just like we did for broadside scanning. The elements (elements: 6, 7 10 and 11) in the middle of the array had reflection co-efficient less than -10 dB for a wide bandwidth of 3.1-4.7 GHz. The elements on the boundary of the array also had reflection co-efficient less than -10dB for a wide bandwidth of 3.25-4.6GHz.

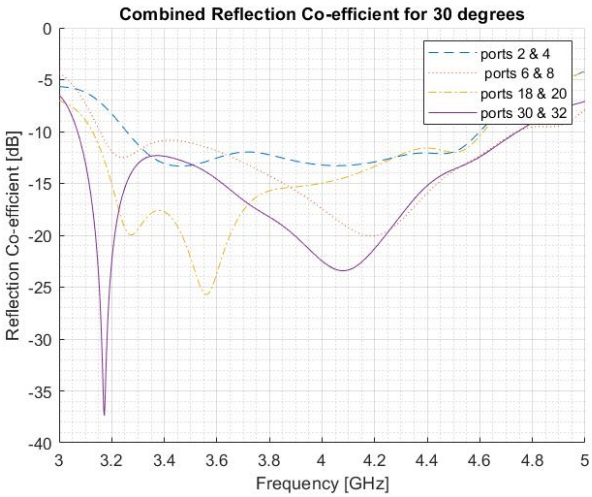

Figure 4.10 Combined reflection co-efficient of the ports of the elements 1, 2, 5 and 6 in the array for scanning ±30° in the E-plane

4.2.4 Individual Port Reflection Co-efficient of Elements in Array for Scanning up to $\pm 45°$ in E-plane

Almost all ports of the array had reflection co-efficient less than -8 dB for the bandwidth 3.2-3.7GHz and this frequency band became slightly narrow for reflection co-efficient less than -10 dB. Elements in the middle of the array (elements: 6, 7 10 and 11), now had three bands for which their reflection co-efficient were less than -10 dB: 3.1-3.2 GHz, 3.4-3.8GHz and 4.5-4.8 GHz. Some elements other than boundary ones, had good reflection co-efficient (less than -10 dB) for higher frequencies band (4.5-4.8 GHz).

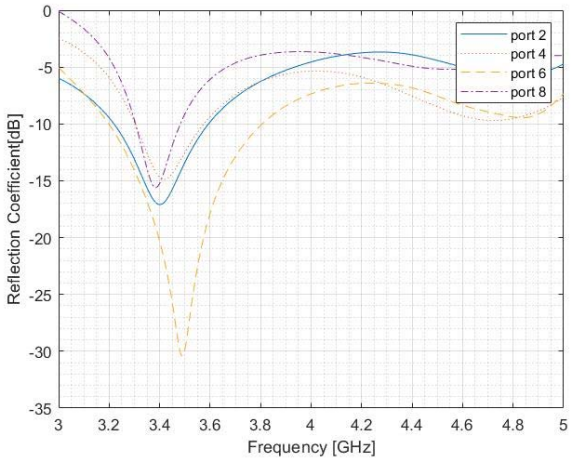

Figure 4.11 Reflection co-efficient of ports 2, 4,6 and 8 in the array for scanning up to $\pm 45°$ in E-plane

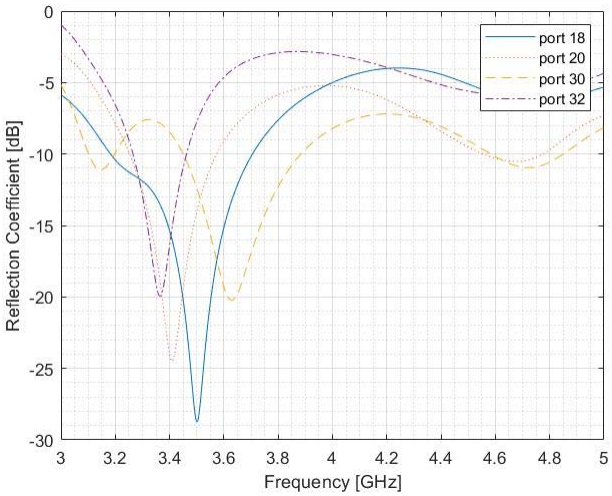

Figure 4.12 Reflection co-efficient of ports 18,20,30 and 32 in the array for scanning up to $\pm 45°$ in E-plane

4.2.5 Combined Reflection Co-efficient of Individual Elements in Array for Scanning up to $\pm 45°$ in E-plane

The elements in the middle of the array had a reflection co-efficient of less than -10dB for a wide bandwidth of 3.1GHz-4 GHz. In this bandwidth, the elements at the boundary of array had a reflection co-efficient of less than -8dB.

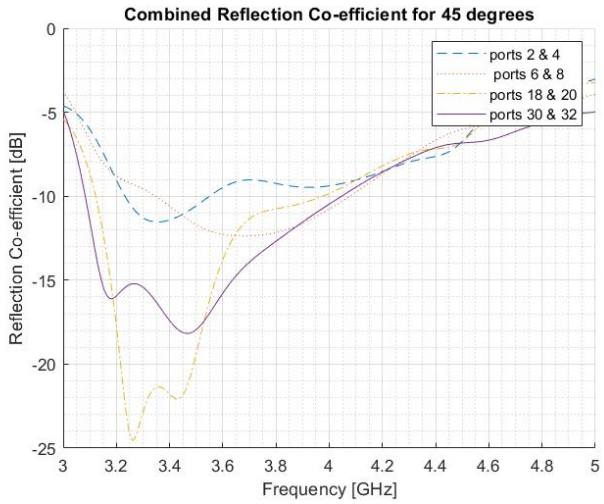

Figure 4.13 Combined reflection co-efficient of the ports for elements 1, 2, 5 and 6 in the array for scanning up to $\pm 45°$ in E-plane

4.2.6 Individual Port Reflection Co-efficient of Elements in Array for Scanning up to $\pm 60°$ E-plane

Almost all elements had reflection co-efficient less than -8dB for the frequency band 3.2- 3.5 GHz. This bandwidth gets narrower by 100 MHz on the both sides for reflection co-efficient less than -10 dB.

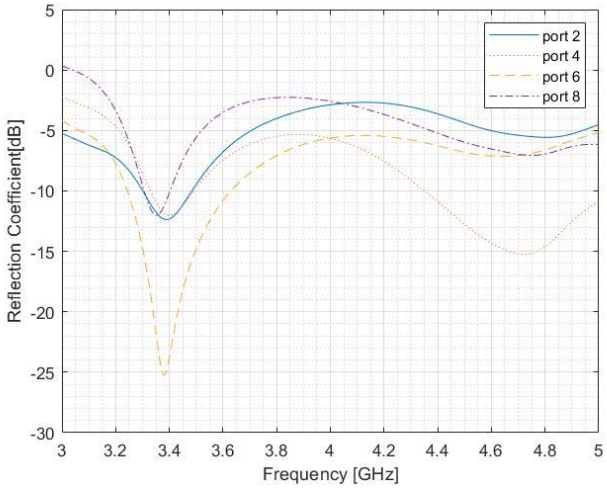

Figure 4.14 Reflection co-efficient of ports 2, 4,6 and 8 in the array for scanning up to $\pm 60°$ in E-plane

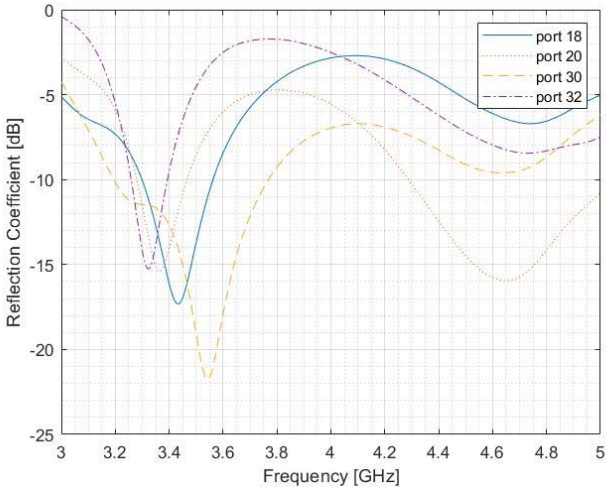

Figure 4.15 Reflection co-efficient of ports 18,20,30 and 32 in the array for scanning up to $\pm 60°$ in E-plane

4.2.7 Combined Reflection Co-efficient of Individual Elements in Array for Scanning up to $\pm 60°$ in E-plane

Elements in the middle of the array had a reflection co-efficient less than -8dB for a frequency band of 3.1-3.6GHz. Corner elements (elements:1, 13, 16 and 4) had poor reflection co-efficient in this bandwidth ($less\ than\ -8dB$). However, elements (elements:2,3, 14 and 15) had a reflection co-efficient less than -8dB for slightly shorter bandwidth: 3.3-3.65 GHz.

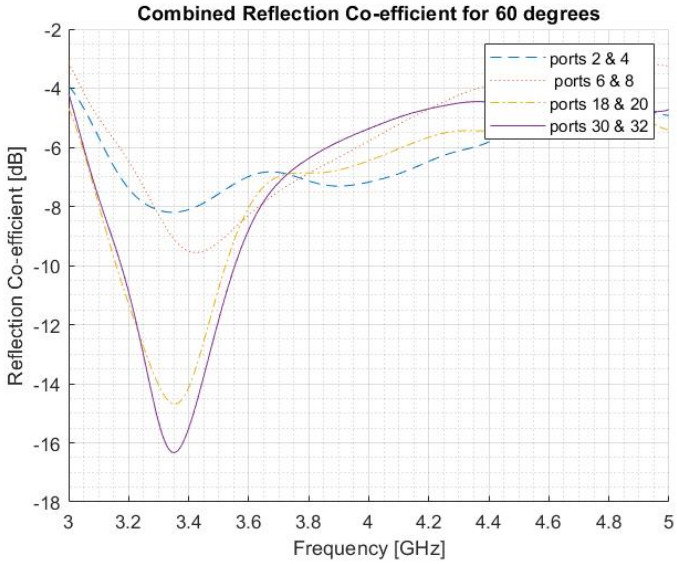

Figure 4.16 Combined reflection co-efficient of the ports for elements 1, 2, 5 and 6 for scanning up to $\pm 60°$ in E-plane

4.2.8 Far-Field Plots of the Array in E-plane:

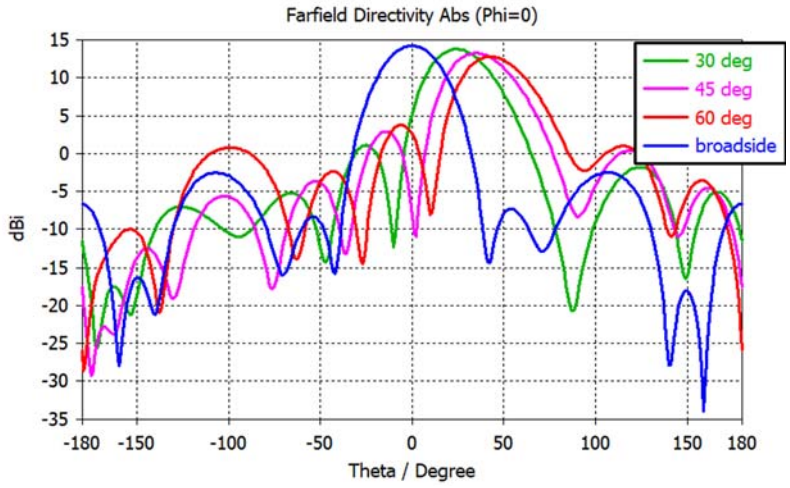

(a)

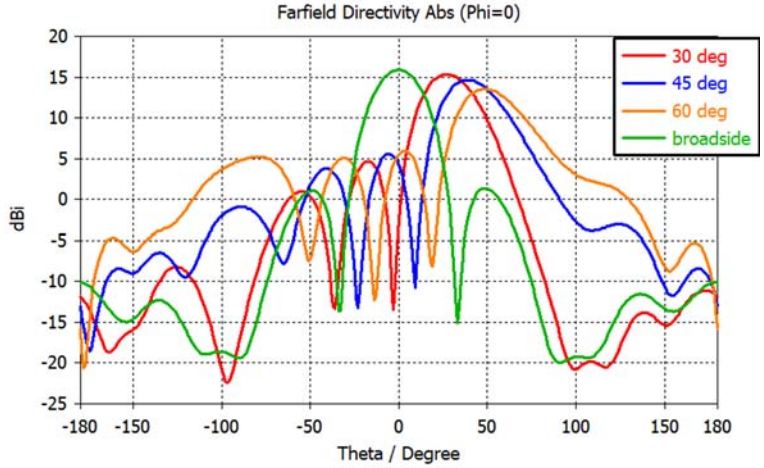

(b)

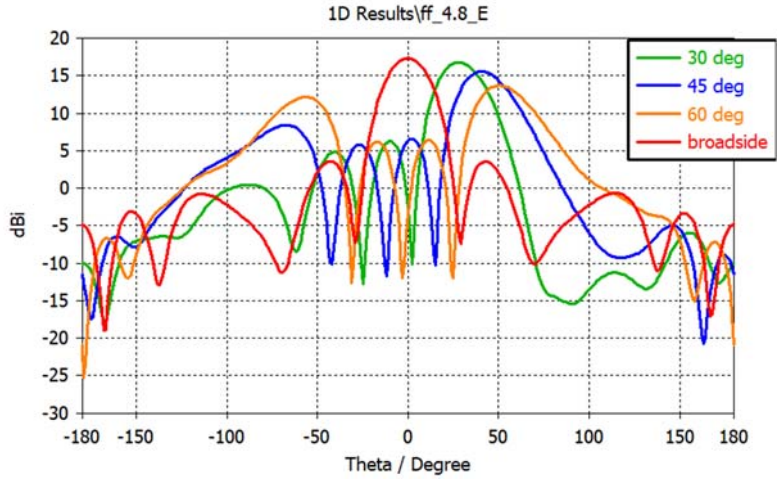

(c)

Figure 4.17 Far-field plots of the array for broadside radiation and scanning up to ±30°, ±45° and ±60° in E-plane for frequencies (a) 3.2 GHz (b) 4 GHz (c) 4.8 GHz.

4.2.9 Individual Port Reflection Co-efficient of Elements in Array for Scanning up to ±30° in H-plane

Elements in the middle of the array (elements: 6, 7 10 and 11 in the Table 4-2 Front view of the 4x4 array showing symmetry for reflection co-efficient for broad scanning for one polarization.), had reflection co-efficient less than -10 dB over the entire bandwidth of 3.2-4.8 GHz. For elements on the boundary of the array (same colored boxed elements as: 1, 2 and 5 in the Table 4-2 Front view of the 4x4 array showing symmetry for reflection co-efficient for broad scanning for one polarization.), had two bandwidths of 3.2-3.8 GHz and 4.5-4.8 GHz for which the reflection co-efficient was less than -8 dB.

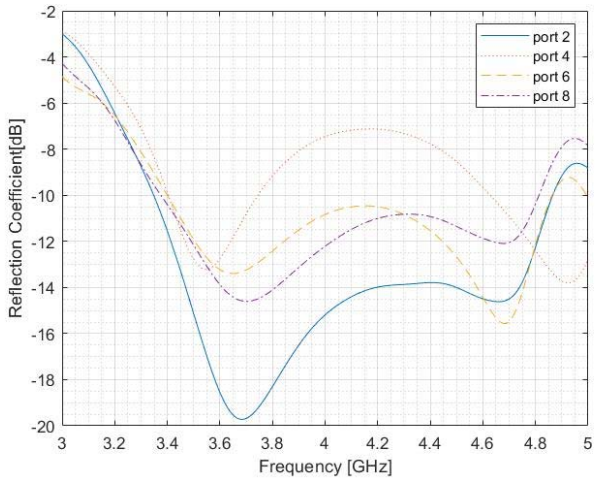

Figure 4.18 Reflection co-efficient of ports 2, 4,6 and 8 for scanning up to ±30° in H-plane

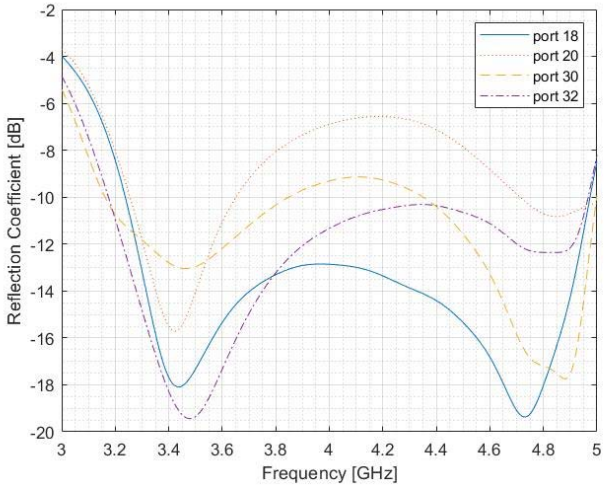

Figure 4.19 Reflection co-efficient of ports 18,20,30 and 32 for scanning ±30°in H-plane

4.2.10 Combined Reflection Co-efficient of Individual Elements in Array for Scanning up to $\pm 30°$ in H-plane

To have combined reflection co-efficient of the pair of ports of each element, we replaced individual waveguide ports with a discrete port. We did this for elements 1, 2, 5 and 6 only, just like we did for broadside scanning.

The elements (elements: 6, 7 10 and 11) in the middle of the array had reflection co-efficient less than -10 dB for a wide bandwidth of 3.25- 4.8 GHz. The elements on the corner of the array also reflection co-efficient less than -10dB for a bandwidth of 3.6-4.8 GHz. Some boundary elements (elements 3,2,14 and 15) had slightly narrow bandwidth of 4-4.8 GHz for reflection co-efficient less than -10 dB. While boundary elements like (elements:8, 12,9 and 15) had wide bandwidth of 3.25- 4.8 GHz for reflection-co-efficient less than -10 dB.

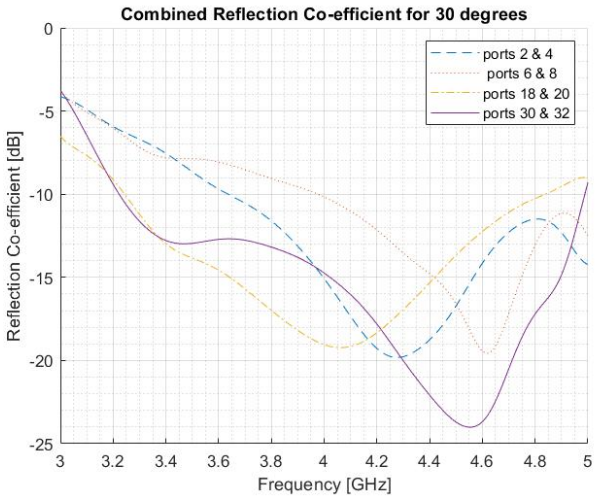

Figure 4.20 Combined reflection co-efficient of the ports for elements 1, 2, 5 and 6 for scanning up to $\pm 30°$ in H-plane

4.2.11 Individual Port Reflection Co-efficient of Elements in Array for Scanning up to $\pm 45°$ in H-plane

Almost all elements of the array had reflection co-efficient less than -8 dB for the bandwidth 3.3-3.6 GHz and this frequency band became slightly narrow for reflection co-efficient less than -10 dB.

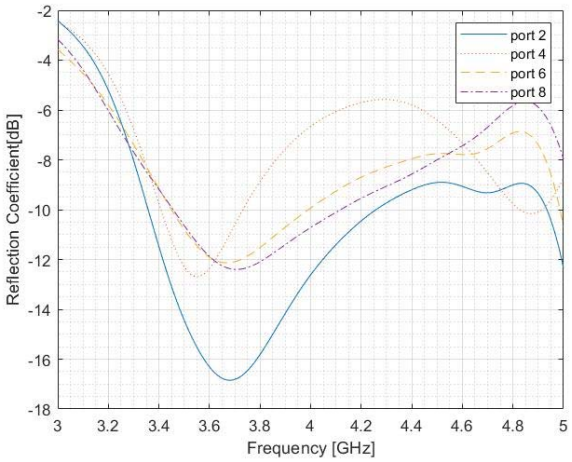

Figure 4.21 Reflection co-efficient of ports 2, 4,6 and 8 scanning up to ±45° in H-plane

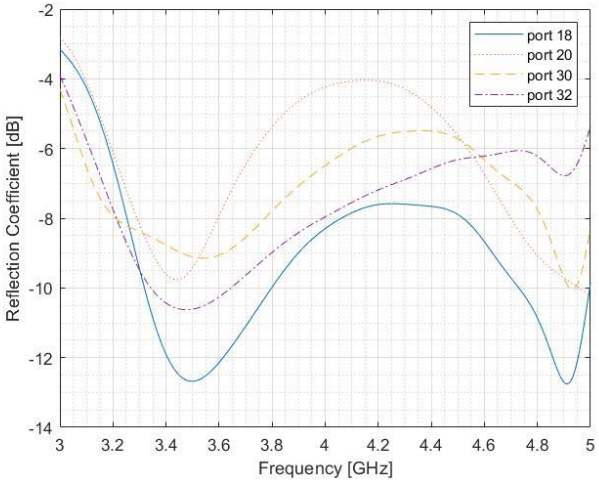

Figure 4.22 Reflection co-efficient of ports 18,20,30 and 32 scanning up to ±45° in H-plane

4.2.12 Combined Reflection Co-efficient of Individual Elements in Array for Scanning up to $\pm 45°$ in H-plane

The elements in the middle of the array had a reflection co-efficient of less than -8dB for a bandwidth of 3.2GHz-3.48 GHz and 4.4-4.8GHz. Elements on the boundary of the array had a better reflection co-efficient than the middle ones. The corner elements had reflection co-efficient of less than -10 dB for a bandwidth of 3.6-4.8 GHz.

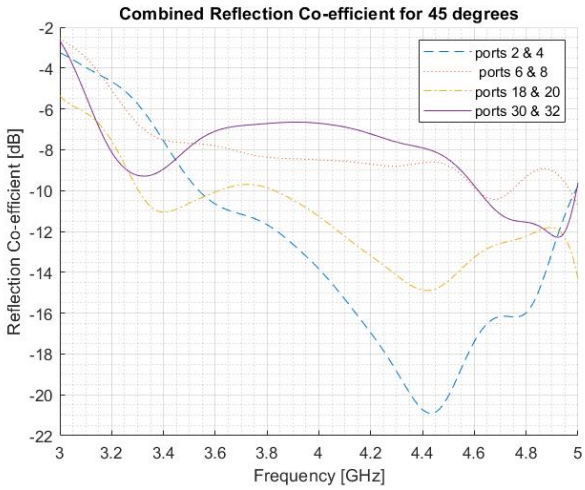

Figure 4.23 Combined reflection co-efficient of the ports for elements 1, 2, 5 and 6 for scanning up to ±45° in H-plane

4.2.13 Individual Port Reflection Co-efficient of Elements in Array for Scanning up to ±60° in H-plane

Only a few elements had reflection co-efficient less than -8dB for the frequency band 3.37GHz-3.8GHz.

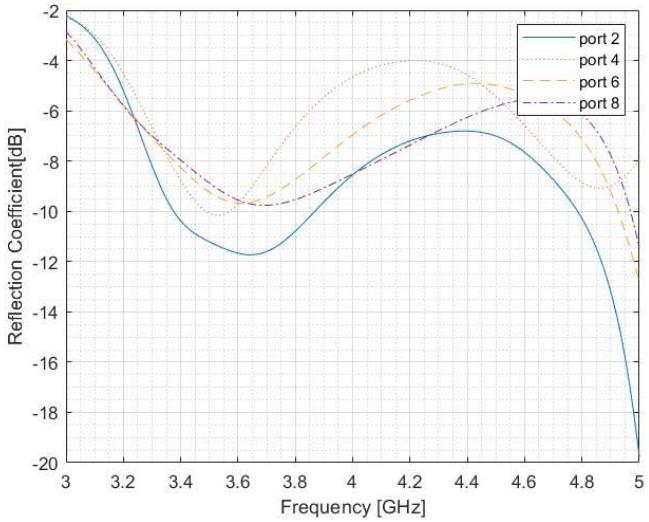

Figure 4.24 Reflection co-efficient of ports 2, 4,6 and 8 for scanning up to ±60° in H-plane

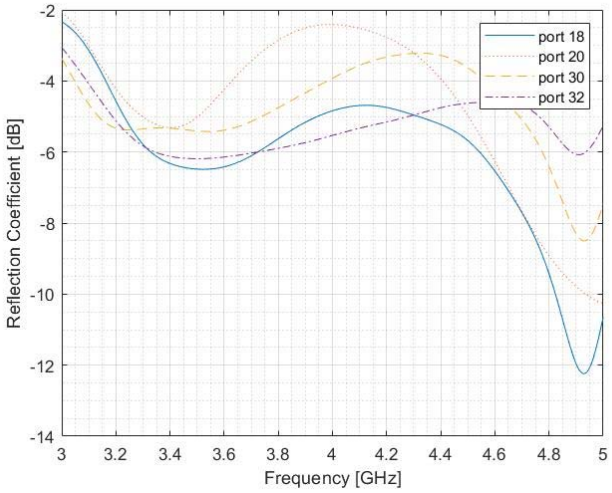

Figure 4.25 Reflection co-efficient of ports 18,20,30 and 32 for scanning up to ±60° in H-plane

4.2.14 Combined Reflection Co-efficient of Individual Elements in Array for Scanning up to ±60° in H-plane

Only the corner elements (elements:1, 13, 16 and 4) had a reflection co-efficient better than -8dB for a frequency band of 3.36-4.85 GHz.

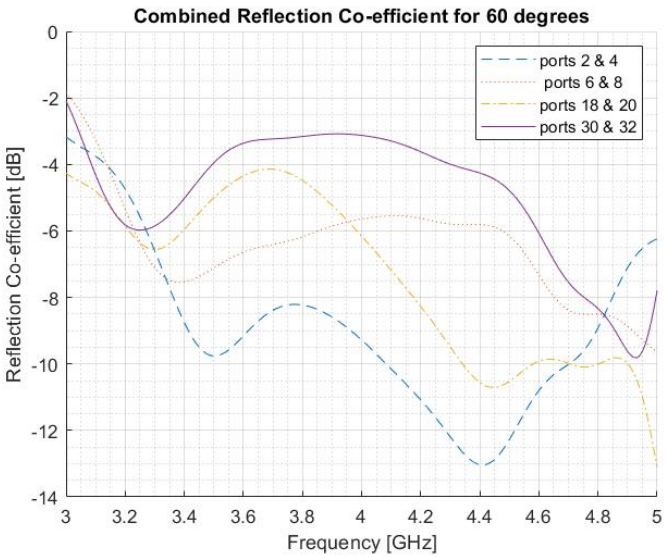

Figure 4.26 Combined reflection co-efficient of the ports for elements 1, 2, 5 and 6 for scanning up to ±60° in H-plane.

4.2.15 Far-Field Plots of the Array in H-Plane:

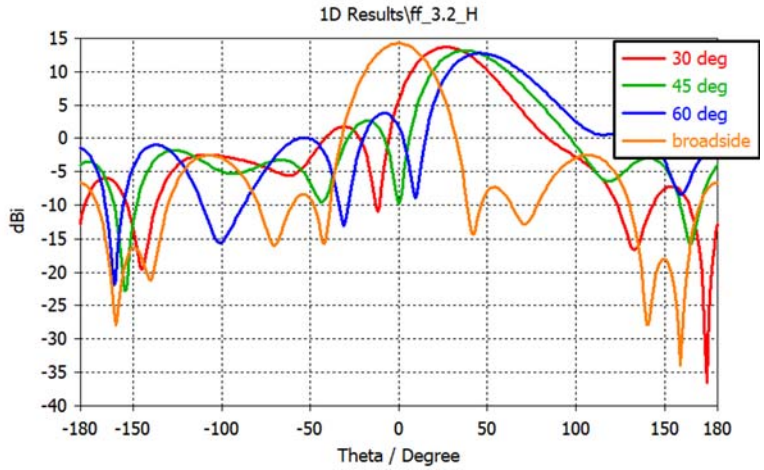

(a)

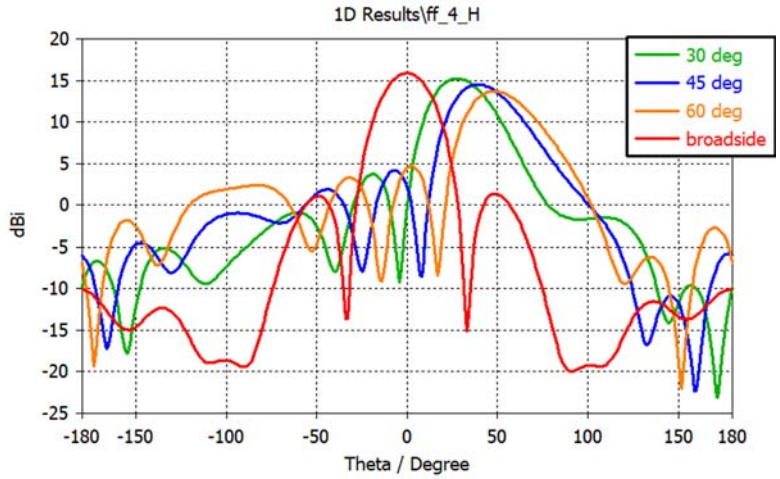

(b)

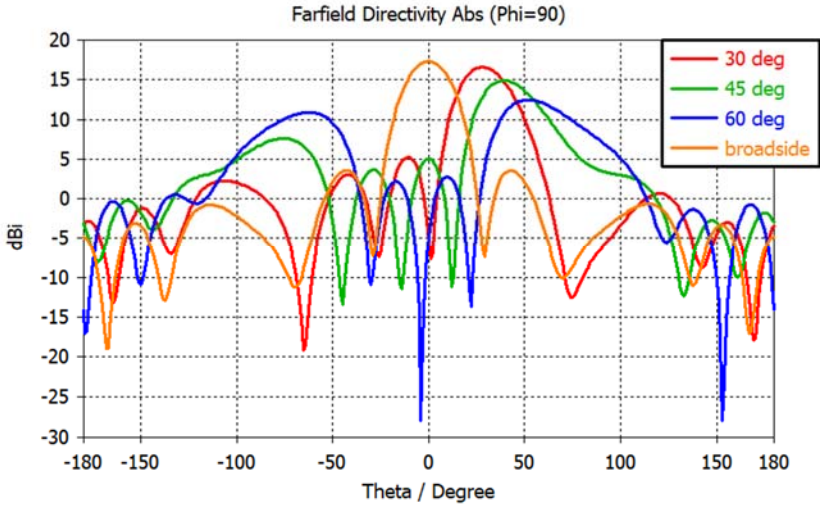

(c)

Figure 4.27 Far-field plots of the array for broadside radiation and scanning up to ±30°, ±45° and ±60° in H-plane for frequencies (a) 3.2 GHz (b) 4 GHz (c) 4.8 GHz.

5 DISSCUSSION

In this thesis work, a manufacturable compact wide band, *4 by 4* dual-polarized phased-array self-grounded bowtie antenna had been designed and the simulation results had been analyzed for sub-6GHz. The single element was designed and modelled for an array configuration. In the broadside direction it had a reflection co-efficient better than -15 dB for both polarizations and the far-field radiation patterns were stable with a directivity of 14.3-17.8 dBi over the desired bandwidth 3.1-4.8 GHz. As the main beam of the single element scanned up to ±60°, the reflection co-efficient was compromised. This could be due to the reason that the single element was optimized mainly in the broadside direction only. However, grating lobes in the far-field radiation patterns do not start appearing until the degree of scanning is ±60° for frequencies higher than 4.4 GHz.

The array antenna was analyzed for both polarizations in both planes. The E-plane of one polarization corresponded to the H-plane of the other polarizations. This meant that result of one polarization in E- would be same as H-plane results of the other polarization. Therefore, this report only contains simulation results of one polarization in both planes.

The array antenna had a directivity range of 14.2- 17.3 dBi, 13.2-16.8 dBi, 13.6-15.7 dBi and 12.7-13.7 dBi over the bandwidth of 3.2-4.8 GHz for broadside radiation, ±30°, ±45° and ±60° scanning, respectively, in both planes. Grating lobes do not appear until the main beam scanning is performed for ±60° for frequencies higher than 4.2 GHz and this is because the element spacing criteria to avoid grating lobes for scanning up to ±60° was met while designing the element. In the broadside direction, all the elements have a reflection co-efficient better than -15 dB over the bandwidth. However, the reflection co-efficient of the elements ports in the array was compromised the most when the degree of the scanning is increased up to ±60° . This is because no optimization of the array for different scanning was performed. The array antenna showed different performance in terms of reflection co-efficient in both E- and H-planes for a polarization.

5.1 Further Improvements and Future Work

In this thesis work, the element was optimized for broadside direction only over the bandwidth and no optimization was performed for the different scanning. One area of improvement could be to optimize the element for different scanning as well. In this way the element could perform better in different degrees of scanning without showing drastic changes in the performance.

Optimization of the single element was done to achieve the required specifications. However, no optimization of the complete array antenna was performed in this thesis work. Another area of improvement and as well further work could be to optimize the complete array antenna to give better performance at higher degrees of scanning's. One idea could be to optimize the elements on the boundary primarily at scanning of ±25°. This will not only improve the overall

array performance, but the array will not show sudden degradation while scanning from broadside to scanning up to 25°.

As for future work, measurement and validation of the array antenna prototype could be performed. Moreover, analysis of this array antenna could be performed in in a real scenario such in a massive 5G MIMO system.

5.2 Potential Applications

This antenna was designed to be used for the MIMO system in wireless communications. Nevertheless, the antenna, as it can offer all the benefits of the phased array antennas, it can be used for different applications as well. Phased array antennas are a very popular choice of antenna in the airborne and ground based wireless communication and radar applications.

In wireless communications, they can overcome the problems of limited channel bandwidth and reduce the problems of multipath fading, and co-channel interference. When used along with MIMO systems at the base station, they help to utilize the frequency spectrum more efficiently and provide higher date rates and accommodate large number of users at the same time. Multiple beam forming, and steering can provide the benefit for higher coverage in the wireless communications. By steering multiple beams in different directions and tailoring beam shape, many mobile users can be accommodated.

Other than that, they can have applications in radar-based systems like remote sensing and air surveillance. They can also be used in ground traffic control by the traffic police to control and monitor traffic. In military, they can be used for target detection. They can cancel out interference from different directions. And have an ability to determine the direction of the arrival of the signal.

5.3 Conclusion

A detailed literature study was done on the basic concepts of antenna and different published papers on self-grounded bowtie antenna were conferred. Different modelling techniques were studied and applied on the design of the dual-polarized self-grounded bowtie antenna element which was optimized for an array configuration (N ×N). An array of 4×4 of dual-polarized self-grounded bowtie antenna was designed and analyzed for sub-6GHz with an aim to manufacture a prototype.

The simulation results of the array showed a reflection co-efficient better than -8 dB, for main beam steering up to $\pm 45°$, in the bandwidth of 3.1-4.8 GHz and 3.3-3.6 GHz in E-plane and H-plane respectively. The radiation patterns were stable and directive. The side-lobe levels were less than -7 dB than the main beam with no grating lobes while scanning up to $\pm 45°$in E- and H-planes. For higher degree of scanning up to $\pm 60°$, the performance of the array antenna is compromised.

Further improvements in the array design and potential applications were also discussed in the report. To manufacture a prototype to further analyze the performance of the array in different scanning's was decided. The prototype can show good performance for scanning up to $\pm 25° - 35°$ or maybe more but the prototype needs to be tested before further conclusions can be drawn on the array performance.

References

[1] N. T. Huong, L. T. Trung and N. Q. Dinh, "Proposal of Two Ultra-wide Band Antennas for UWB-MIMO," in *Third World Congress on Information and Communication Technologies (WICT 2013)*, Hanoi, 2013.

[2] P.Kildal, *"Foundations of Antenna Engineering: a Unified Approach for Line of Sight and Multipath"*, Kildal Antenna AB, 2015.

[3] D. M. Pozar, "*Microwave Engineering"*, 4th, Ed., 2005.

[4] S. J.Orfandis, "*Electromagnetic Waves and Antenna"s*, 2016.

[5] S. Jeon and C.-H. Ahn, "Resistive and Inductive Loading Techniques on Microstrip Antenna for Wideband Application," *Journal of Electrical Engineering & Technology*, vol. 6, no. 5, p. . 693~696, 2011.

[6] S. Emami, "U*WB Communication Systems: Conventional and 60 GHz: Principles, Design and Standards"*, Springer, 2013.

[7] C. Jeon and Y. D. Chung, "*Communication Systems"*, 2005.

[8] M. C. Ezuma, S. Subedi, and J. Pyun, “Design of a Compact UWB Antenna for Multi-band Wireless Applications”,in *International Conference on Information Networking (ICOIN)*, Cambodia, 2015.

[9] J. Yang and A. Kishk, "A Novel Low-Profile Compact Directional Ultra-Wideband Antenna: The Self-Grounded Bow-Tie Antenna," *IEEE Transactions on Antennas and Propagation*, vol. 60, no. 3, pp. 1214-1220, 2012.

[10] O. Haraz and A.-R. Sebak, "*UWB Antennas for Wireless Applications"*, 2002.

[11] Y. Zhao and W. Hu, "Design of a UWB Unidirectional Radiation Compound Spiral Antenna," in *2015 IEEE 6th International Symposium on Microwave, Antenna, Propagation, and EMC Technologies, MAPE 2015*, 2016.

[12] Y. L. Dai, B. Yuan, X. H. Zhang, X. W. Dai and G. Q. Luo, "A Novel Compact Ultra-wideband Metamaterial-Based Microstrip Antenna," in *IEEE*, 2016.

[13] X. Huang, C. Cheng and L. Zhu, "Wideband Antenna using a Multiple-mode Slotline Radiator: Proposal and Implementation," *IET Microwaves, Antennas & Propagation*, vol. 5, no. 14, pp. 1773-1778, 2011.

[14] J. Yang and A. Kishk, "The self-grounded Bow-Tie antenna," *IEEE Antennas and Propagation Society, AP-S International Symposium (Digest)*, pp. 1452-1455, 2011.

[15] J. Yang, H. Raza, A. Hussain and P.-S. Kidal, "Wideband compact 4-port dual polarized self-grounded bowtie antenna, IEEE Trans. Antennas Propag., vol. 62, no. 9, pp. 4468–4473, 2014.

[16] A. Al-Ravi, J. Yang, C. Orlenius and M. Franzen, "The double-sided 4-port bow-tie antenna: A new compact wideband MIMO antenna," in *Antennas and Propagation (EuCAP)*, 2013.

[17] J. Yang, P.-S. Kildal, S. M. Moghaddam and A. . A. Glazunov, "Wideband Dual-Polarized Linear Array Antenna For Random-LOS OTA Measurement".

[18] S. M. Moghaddam, J. Yang, P.-S. Kildal and A. A. Glazunov1, "Designing a Dual-Polarized Octave Bandwidth Bowtie Antenna for a Linear Array," in *10th European Conference on Antennas and Propagation, EuCAP 2016*.

[19] S. Abtah, J. Yang and S. Kidborg, "A New Compact Multiband Antenna for Stroke Diagnosis System over 0.5-3 GHz," *Microwave and Optical Technology Lett.*, vol. 54, no. 10, p. 2342–2346, October 2012.

[20] Q. Jian and J. Yang, "Detection of Breathing and Heartbeat by Using a Simple UWB Radar System," in *8th European Conference on Antennas and Propagation, EuCAP 2014*, 2014.

APPENDIX

Far-field plot- 3D

ELEMENT

BROADSIDE:

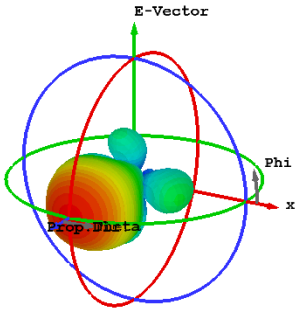

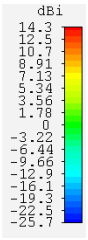

Type	Farfield (Array)
Approximation	enabled (kR >> 1)
Monitor	farfield (f=3.2) [1(1)]
Component	Abs
Output	Directivity
Frequency	3.2 GHz
Rad. effic.	-0.01906 dB
Tot. effic.	-0.1545 dB
Dir.	14.25 dBi

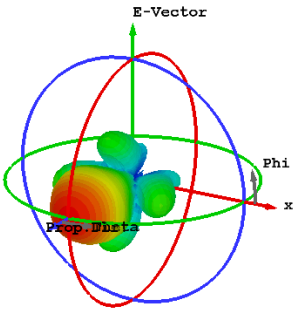

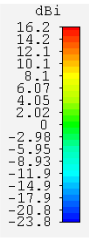

Type	Farfield (Array)
Approximation	enabled (kR >> 1)
Monitor	farfield (f=4) [1(1)]
Component	Abs
Output	Directivity
Frequency	4 GHz
Rad. effic.	-0.01591 dB
Tot. effic.	-0.2078 dB
Dir.	16.19 dBi

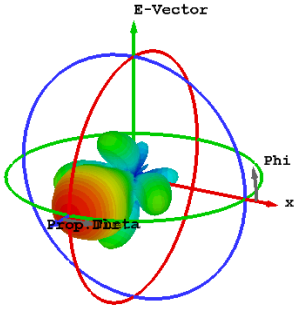

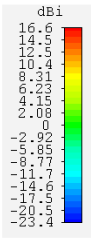

Type	Farfield (Array)
Approximation	enabled (kR >> 1)
Monitor	farfield (f=4.2) [1(1)]
Component	Abs
Output	Directivity
Frequency	4.2 GHz
Rad. effic.	-0.01653 dB
Tot. effic.	-0.1974 dB
Dir.	16.61 dBi

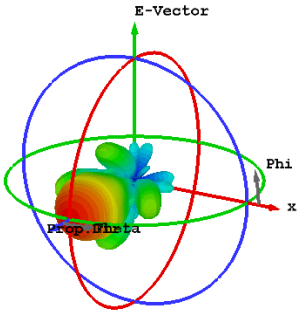

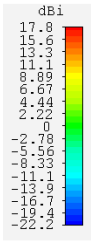

Type	Farfield (Array)
Approximation	enabled (kR >> 1)
Monitor	farfield (f=4.8) [1(1)]
Component	Abs
Output	Directivity
Frequency	4.8 GHz
Rad. effic.	-0.02453 dB
Tot. effic.	-0.06959 dB
Dir.	17.78 dBi

ELEMENT-±30° SCANNING-E-plane

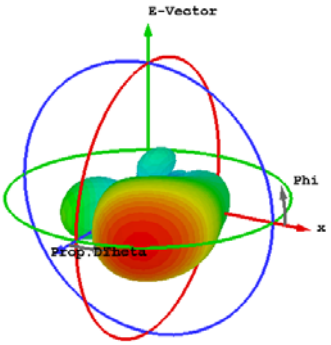

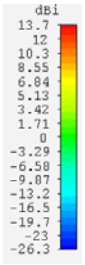

Type	Farfield (Array)
Approximation	enabled (kR >> 1)
Monitor	farfield (f=3.2) [1(1)]
Component	Abs
Output	Directivity
Frequency	3.2 GHz
Rad. effic.	-0.01924 dB
Tot. effic.	-0.2602 dB
Dir.	13.68 dBi

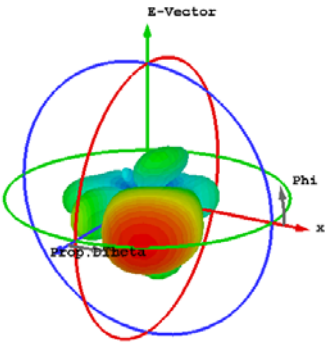

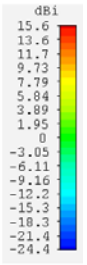

Type	Farfield (Array)
Approximation	enabled (kR >> 1)
Monitor	farfield (f=4) [1(1)]
Component	Abs
Output	Directivity
Frequency	4 GHz
Rad. effic.	-0.01271 dB
Tot. effic.	-0.3670 dB
Dir.	15.57 dBi

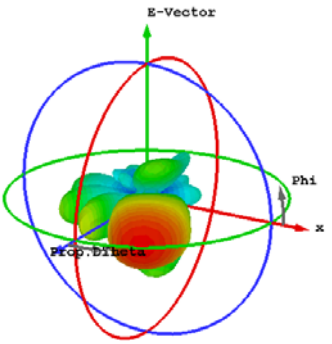

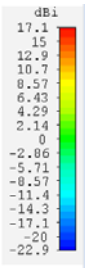

Type	Farfield (Array)
Approximation	enabled (kR >> 1)
Monitor	farfield (f=4.8) [1(1)]
Component	Abs
Output	Directivity
Frequency	4.8 GHz
Rad. effic.	-0.01877 dB
Tot. effic.	-0.06672 dB
Dir.	17.14 dBi

ELEMENT-±30° SCANNING-H-plane

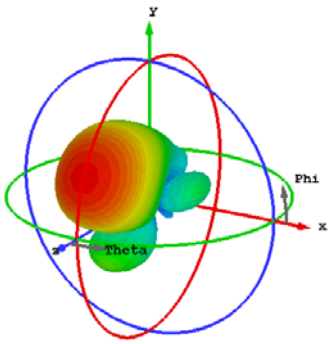

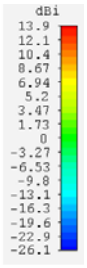

Type	Farfield (Array)
Approximation	enabled (kR >> 1)
Monitor	farfield (f=3.2) [1(1)]
Component	Abs
Output	Directivity
Frequency	3.2 GHz
Rad. effic.	-0.03072 dB
Tot. effic.	-0.4835 dB
Dir.	13.88 dBi

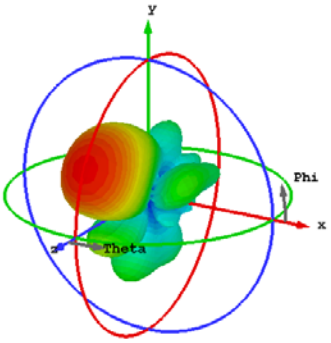

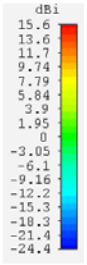

Type	Farfield (Array)
Approximation	enabled (kR >> 1)
Monitor	farfield (f=4) [1(1)]
Component	Abs
Output	Directivity
Frequency	4 GHz
Rad. effic.	-0.05607 dB
Tot. effic.	-0.5702 dB
Dir.	15.58 dBi

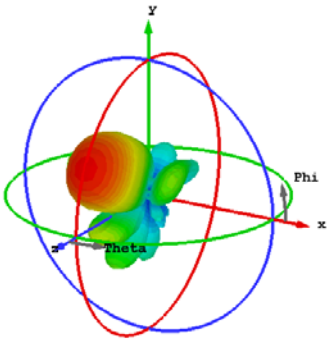

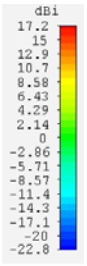

Type	Farfield (Array)
Approximation	enabled (kR >> 1)
Monitor	farfield (f=4.8) [1(1)]
Component	Abs
Output	Directivity
Frequency	4.8 GHz
Rad. effic.	-0.02474 dB
Tot. effic.	-0.1405 dB
Dir.	17.18 dBi

ELEMENT-45° SCANNING-E-plane

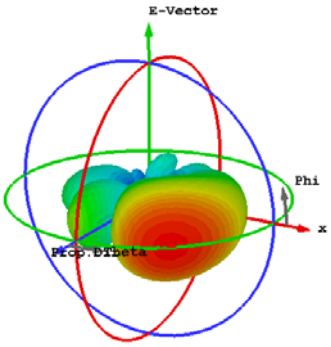

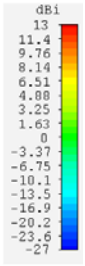

Type	Farfield (Array)
Approximation	enabled (kR >> 1)
Monitor	farfield (f=3.2) [1(1)]
Component	Abs
Output	Directivity
Frequency	3.2 GHz
Rad. effic.	-0.02823 dB
Tot. effic.	-0.5703 dB
Dir.	13.02 dBi

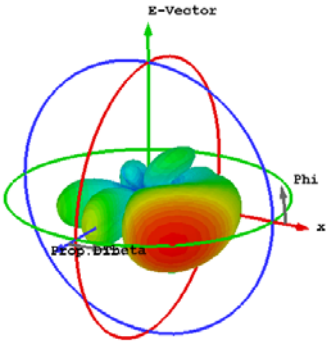

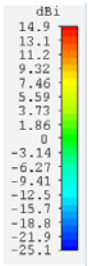

Type	Farfield (Array)
Approximation	enabled (kR >> 1)
Monitor	farfield (f=4) [1(1)]
Component	Abs
Output	Directivity
Frequency	4 GHz
Rad. effic.	-0.01952 dB
Tot. effic.	-0.8087 dB
Dir.	14.92 dBi

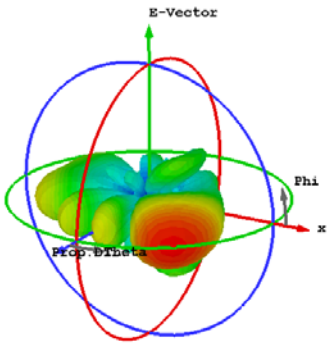

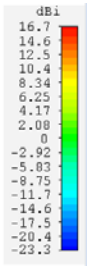

Type	Farfield (Array)
Approximation	enabled (kR >> 1)
Monitor	farfield (f=4.8) [1(1)]
Component	Abs
Output	Directivity
Frequency	4.8 GHz
Rad. effic.	-0.02738 dB
Tot. effic.	-0.5556 dB
Dir.	16.68 dBi

ELEMENT-45° SCANNING-H-plane

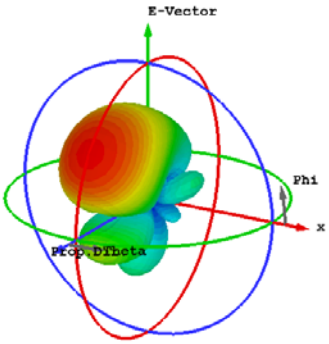

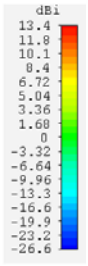

Type	Farfield (Array)
Approximation	enabled (kR >> 1)
Monitor	farfield (f=3.2) [1(1)]
Component	Abs
Output	Directivity
Frequency	3.2 GHz
Rad. effic.	-0.04806 dB
Tot. effic.	-1.001 dB
Dir.	13.43 dBi

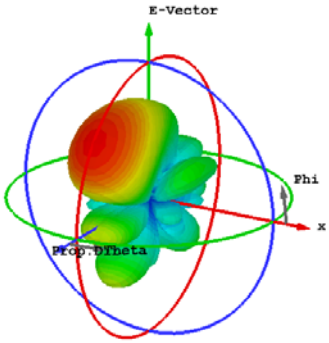

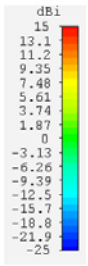

Type	Farfield (Array)
Approximation	enabled (kR >> 1)
Monitor	farfield (f=4) [1(1)]
Component	Abs
Output	Directivity
Frequency	4 GHz
Rad. effic.	-0.07847 dB
Tot. effic.	-1.622 dB
Dir.	14.96 dBi

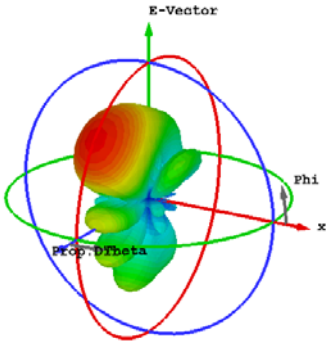

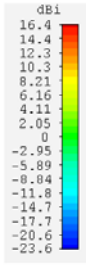

Type	Farfield (Array)
Approximation	enabled (kR >> 1)
Monitor	farfield (f=4.8) [1(1)]
Component	Abs
Output	Directivity
Frequency	4.8 GHz
Rad. effic.	-0.02953 dB
Tot. effic.	-0.3764 dB
Dir.	16.43 dBi

ELEMENT-60° SCANNING-E-plane

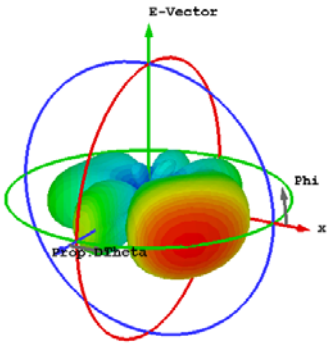

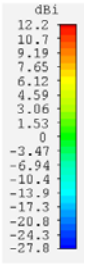

Type	Farfield (Array)
Approximation	enabled (kR >> 1)
Monitor	farfield (f=3.2) [1(1)]
Component	Abs
Output	Directivity
Frequency	3.2 GHz
Rad. effic.	-0.04125 dB
Tot. effic.	-1.338 dB
Dir.	12.25 dBi

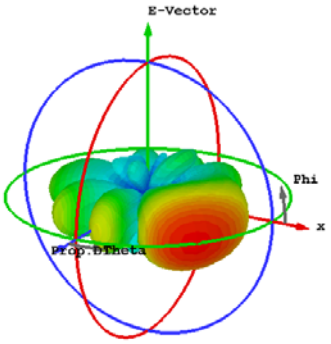

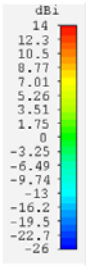

Type	Farfield (Array)
Approximation	enabled (kR >> 1)
Monitor	farfield (f=4) [1(1)]
Component	Abs
Output	Directivity
Frequency	4 GHz
Rad. effic.	-0.02873 dB
Tot. effic.	-1.889 dB
Dir.	14.03 dBi

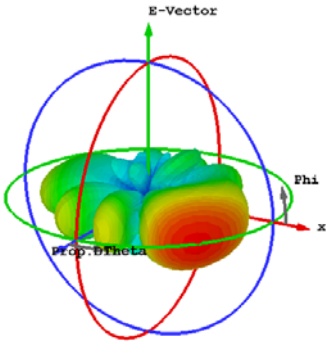

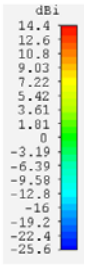

Type	Farfield (Array)
Approximation	enabled (kR >> 1)
Monitor	farfield (f=4.2) [1(1)]
Component	Abs
Output	Directivity
Frequency	4.2 GHz
Rad. effic.	-0.02769 dB
Tot. effic.	-2.099 dB
Dir.	14.45 dBi

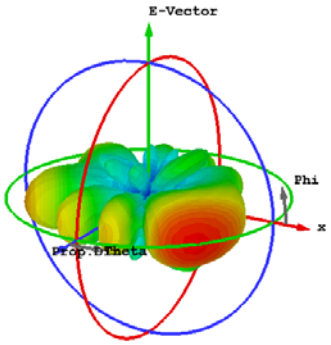

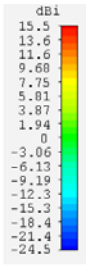

Type	Farfield (Array)
Approximation	enabled (kR >> 1)
Monitor	farfield (f=4.6) [1(1)]
Component	Abs
Output	Directivity
Frequency	4.6 GHz
Rad. effic.	-0.03387 dB
Tot. effic.	-2.314 dB
Dir.	15.49 dBi

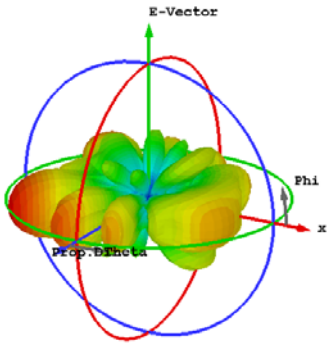

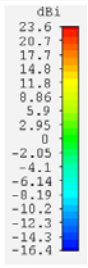

Type	Farfield (Array)
Approximation	enabled (kR >> 1)
Monitor	farfield (f=4.8) [1(1)]
Component	Abs
Output	Directivity
Frequency	4.8 GHz
Rad. effic.	-0.2606 dB
Tot. effic.	-7.544 dB
Dir.	23.82 dBi

ELEMENT-60° SCANNING-H-plane

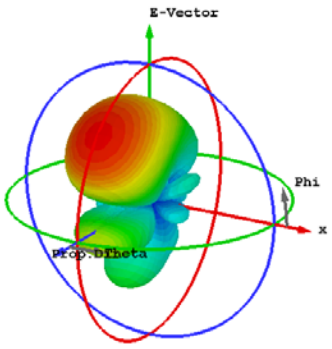

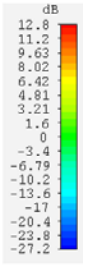

Type	Farfield (Array)
Approximation	enabled (kR >> 1)
Monitor	farfield (f=3.2) [1(1)]
Component	Abs
Output	Gain
Frequency	3.2 GHz
Rad. effic.	-0.05727 dB
Tot. effic.	-1.597 dB
Gain	12.84 dB

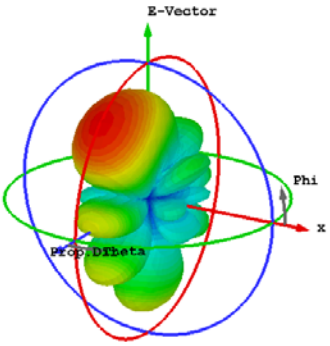

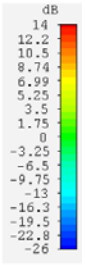

Type	Farfield (Array)
Approximation	enabled (kR >> 1)
Monitor	farfield (f=4) [1(1)]
Component	Abs
Output	Gain
Frequency	4 GHz
Rad. effic.	-0.1100 dB
Tot. effic.	-2.718 dB
Gain	13.89 dB

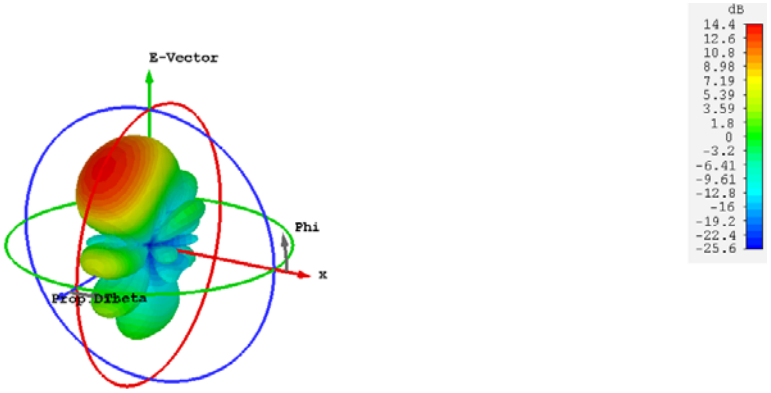

Type	Farfield (Array)
Approximation	enabled (kR >> 1)
Monitor	farfield (f=4.2) [1(1)]
Component	Abs
Output	Gain
Frequency	4.2 GHz
Rad. effic.	-0.03657 dB
Tot. effic.	-0.8991 dB
Gain	14.37 dB

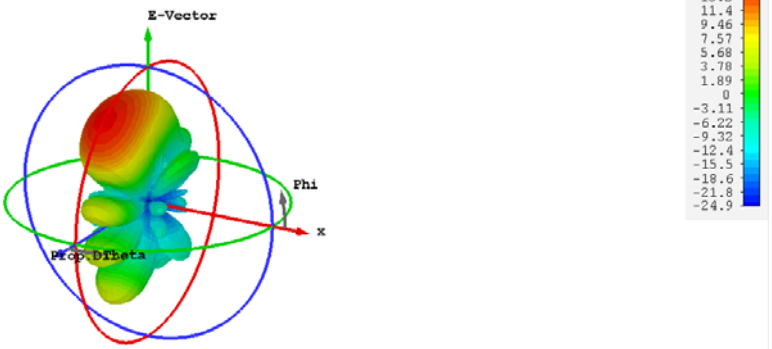

Type	Farfield (Array)
Approximation	enabled (kR >> 1)
Monitor	farfield (f=4.8) [1(1)]
Component	Abs
Output	Gain
Frequency	4.8 GHz
Rad. effic.	-0.03843 dB
Tot. effic.	-0.9189 dB
Gain	15.14 dB

ARRAY_BROADSIDE

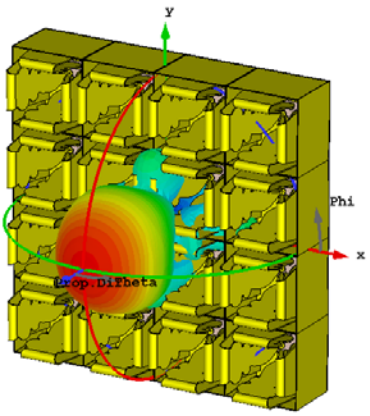

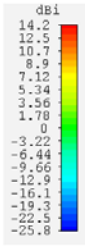

Type	Farfield
Approximation	enabled (kR >> 1)
Monitor	farfield (f=3.2) [broadside_H]
Component	Abs
Output	Directivity
Frequency	3.2 GHz
Rad. effic.	-0.03703 dB
Tot. effic.	-0.8125 dB
Dir.	14.24 dBi

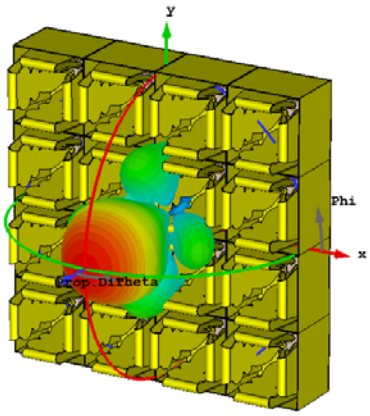

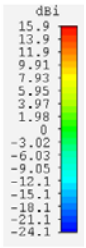

Type	Farfield
Approximation	enabled (kR >> 1)
Monitor	farfield (f=4) [broadside_H]
Component	Abs
Output	Directivity
Frequency	4 GHz
Rad. effic.	-0.01846 dB
Tot. effic.	-0.4619 dB
Dir.	15.86 dBi

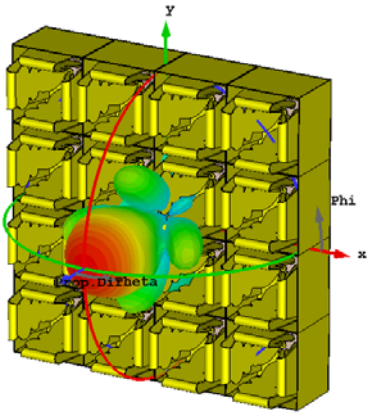

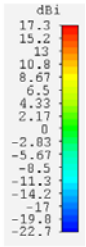

Type	Farfield
Approximation	enabled (kR >> 1)
Monitor	farfield (f=4.8) [broadside_H]
Component	Abs
Output	Directivity
Frequency	4.8 GHz
Rad. effic.	-0.03957 dB
Tot. effic.	-0.2690 dB
Dir.	17.34 dBi

30° Degrees Scanning_E-plane

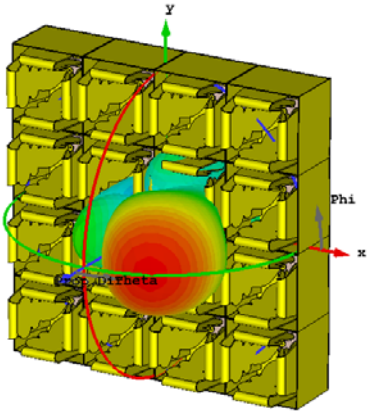

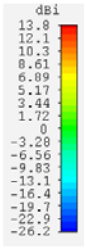

Type	Farfield
Approximation	enabled (kR >> 1)
Monitor	farfield (f=3.2) [SP_30_E]
Component	Abs
Output	Directivity
Frequency	3.2 GHz
Rad. effic.	-0.08048 dB
Tot. effic.	-1.009 dB
Dir.	13.78 dBi

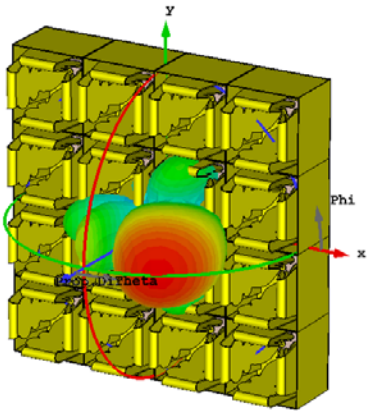

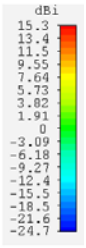

Type	Farfield
Approximation	enabled (kR >> 1)
Monitor	farfield (f=4) [SP_30_E]
Component	Abs
Output	Directivity
Frequency	4 GHz
Rad. effic.	-0.02909 dB
Tot. effic.	-1.006 dB
Dir.	15.28 dBi

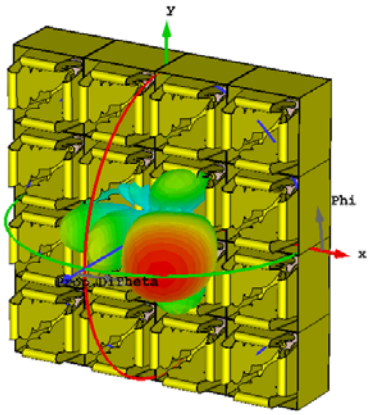

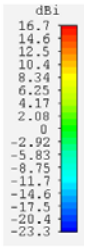

Type	Farfield
Approximation	enabled (kR >> 1)
Monitor	farfield (f=4.8) [SP_30_E]
Component	Abs
Output	Directivity
Frequency	4.8 GHz
Rad. effic.	-0.05201 dB
Tot. effic.	-0.8980 dB
Dir.	16.68 dBi

45° Degrees Scanning_E-plane

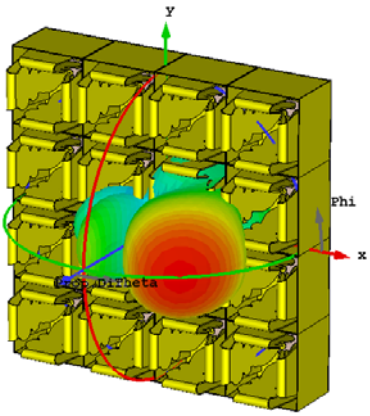

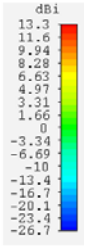

Type	Farfield
Approximation	enabled (kR >> 1)
Monitor	farfield (f=3.2) [SP_45_E]
Component	Abs
Output	Directivity
Frequency	3.2 GHz
Rad. effic.	-0.05769 dB
Tot. effic.	-1.162 dB
Dir.	13.25 dBi

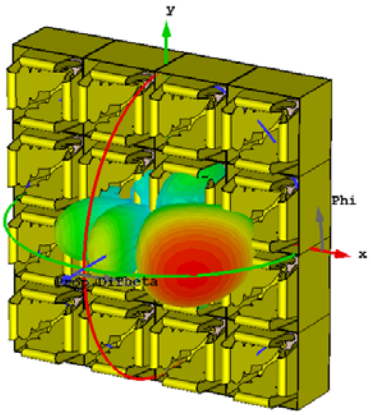

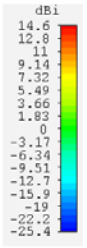

Type	Farfield
Approximation	enabled (kR >> 1)
Monitor	farfield (f=4) [SP_45_E]
Component	Abs
Output	Directivity
Frequency	4 GHz
Rad. effic.	-0.03188 dB
Tot. effic.	-1.557 dB
Dir.	14.63 dBi

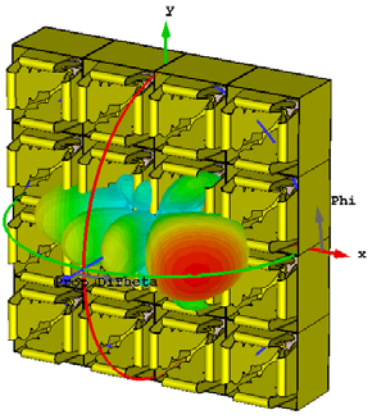

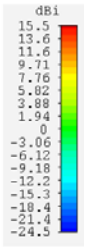

Type	Farfield
Approximation	enabled (kR >> 1)
Monitor	farfield (f=4.8) [SP_45_E]
Component	Abs
Output	Directivity
Frequency	4.8 GHz
Rad. effic.	-0.05079 dB
Tot. effic.	-0.9744 dB
Dir.	15.53 dBi

60° Degrees Scanning-E-Plane

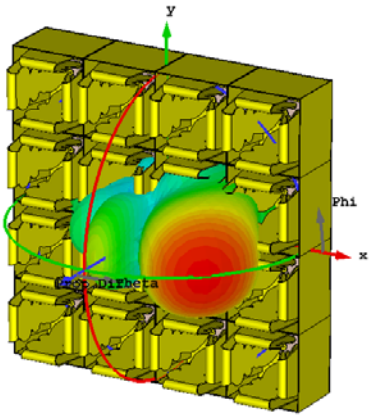

Type	Farfield
Approximation	enabled (kR >> 1)
Monitor	farfield (f=3.2) [SP_60_E]
Component	Abs
Output	Directivity
Frequency	3.2 GHz
Rad. effic.	-0.1153 dB
Tot. effic.	-1.308 dB
Dir.	12.75 dBi

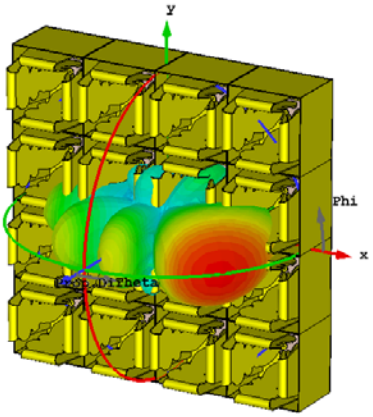

Type	Farfield
Approximation	enabled (kR >> 1)
Monitor	farfield (f=4) [SP_60_E]
Component	Abs
Output	Directivity
Frequency	4 GHz
Rad. effic.	-0.03613 dB
Tot. effic.	-1.944 dB
Dir.	13.50 dBi

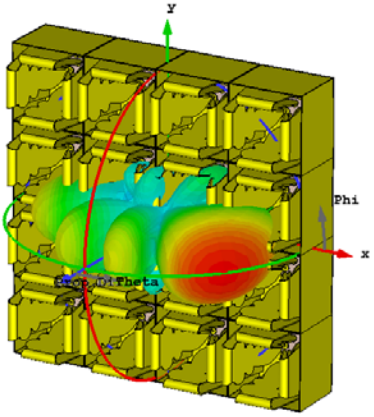

Type	Farfield
Approximation	enabled (kR >> 1)
Monitor	farfield (f=4.2) [SP_60_E]
Component	Abs
Output	Directivity
Frequency	4.2 GHz
Rad. effic.	-0.03370 dB
Tot. effic.	-1.587 dB
Dir.	13.53 dBi

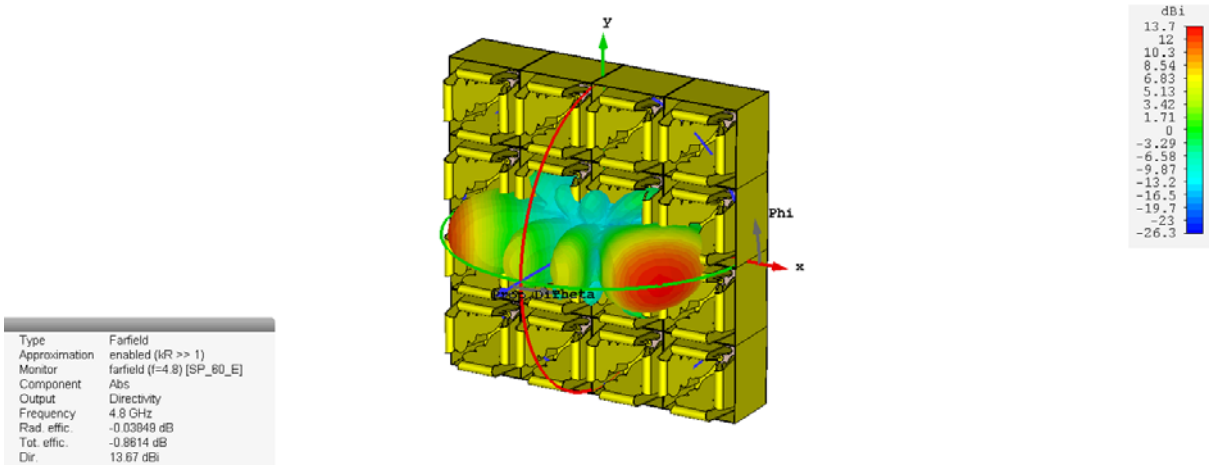
dBi
13.7
12
10.3
8.54
6.83
5.13
3.42
1.71
0
-3.29
-6.58
-9.87
-13.2
-16.5
-19.7
-23
-26.3
y
Phi
x
Type Farfield
Approximation enabled (kR >> 1)
Monitor farfield (f=4.8) [SP_60_E]
Component Abs
Output Directivity
Frequency 4.8 GHz
Rad. effic. -0.03848 dB
Tot. effic. -0.8614 dB
Dir. 13.67 dBi

30° Degrees Scanning-H-Plane

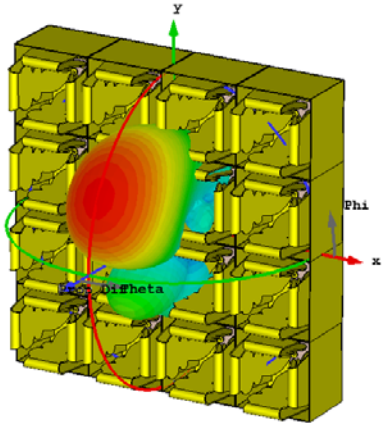

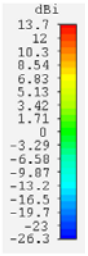

Type	Farfield
Approximation	enabled (kR >> 1)
Monitor	farfield (f=3.2) [SP_30_H]
Component	Abs
Output	Directivity
Frequency	3.2 GHz
Rad. effic.	-0.03924 dB
Tot. effic.	-0.7671 dB
Dir.	13.67 dBi

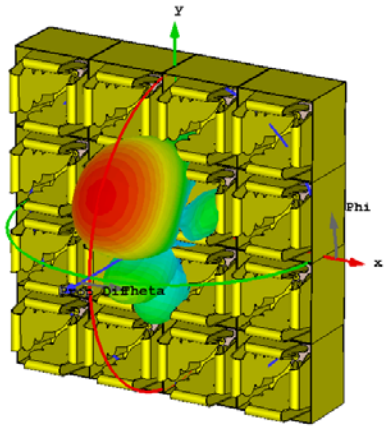

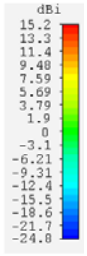

Type	Farfield
Approximation	enabled (kR >> 1)
Monitor	farfield (f=4) [SP_30_H]
Component	Abs
Output	Directivity
Frequency	4 GHz
Rad. effic.	-0.02061 dB
Tot. effic.	-0.6374 dB
Dir.	15.17 dBi

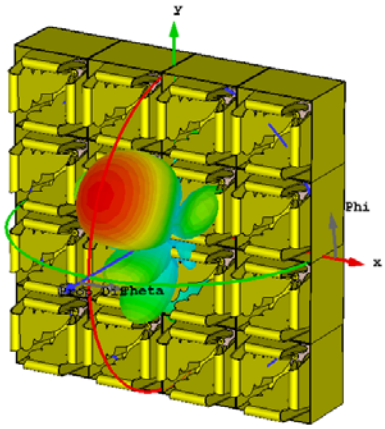

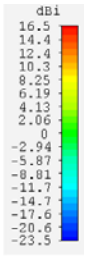

Type	Farfield
Approximation	enabled (kR >> 1)
Monitor	farfield (f=4.8) [SP_30_H]
Component	Abs
Output	Directivity
Frequency	4.8 GHz
Rad. effic.	-0.03432 dB
Tot. effic.	-0.3749 dB
Dir.	16.51 dBi

45° Degrees Scanning-H-Plane

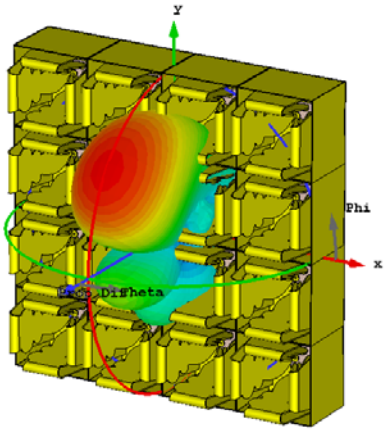

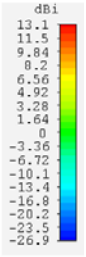

Type	Farfield
Approximation	enabled (kR >> 1)
Monitor	farfield (f=3.2) [SP_45_H]
Component	Abs
Output	Directivity
Frequency	3.2 GHz
Rad. effic.	-0.05488 dB
Tot. effic.	-1.368 dB
Dir.	13.13 dBi

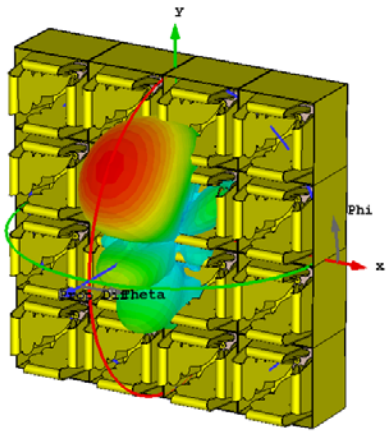

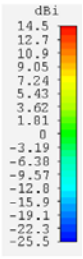

Type	Farfield
Approximation	enabled (kR >> 1)
Monitor	farfield (f=4) [SP_45_H]
Component	Abs
Output	Directivity
Frequency	4 GHz
Rad. effic.	-0.02113 dB
Tot. effic.	-1.157 dB
Dir.	14.49 dBi

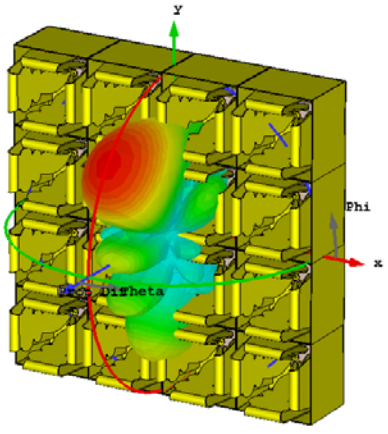

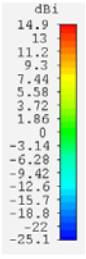

Type	Farfield
Approximation	enabled (kR >> 1)
Monitor	farfield (f=4.8) [SP_45_H]
Component	Abs
Output	Directivity
Frequency	4.8 GHz
Rad. effic.	-0.04331 dB
Tot. effic.	-0.7448 dB
Dir.	14.87 dBi

60° Degrees Scanning-E-Plane

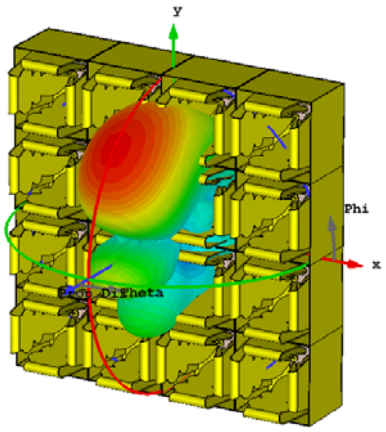

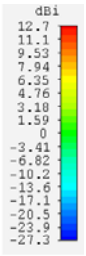

Type	Farfield
Approximation	enabled (kR >> 1)
Monitor	farfield (f=3.2) [SP_60_H]
Component	Abs
Output	Directivity
Frequency	3.2 GHz
Rad. effic.	-0.07507 dB
Tot. effic.	-2.381 dB
Dir.	12.70 dBi

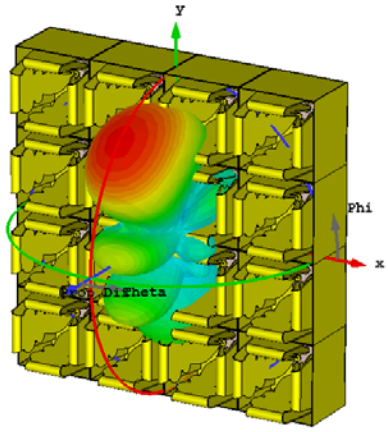

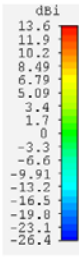

Type	Farfield
Approximation	enabled (kR >> 1)
Monitor	farfield (f=4) [SP_60_H]
Component	Abs
Output	Directivity
Frequency	4 GHz
Rad. effic.	-0.02681 dB
Tot. effic.	-2.118 dB
Dir.	13.58 dBi

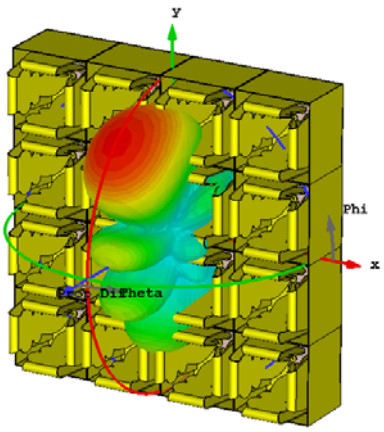

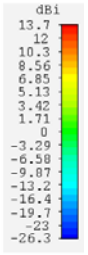

Type	Farfield
Approximation	enabled (kR >> 1)
Monitor	farfield (f=4.2) [SP_60_H]
Component	Abs
Output	Directivity
Frequency	4.2 GHz
Rad. effic.	-0.02500 dB
Tot. effic.	-2.165 dB
Dir.	13.69 dBi

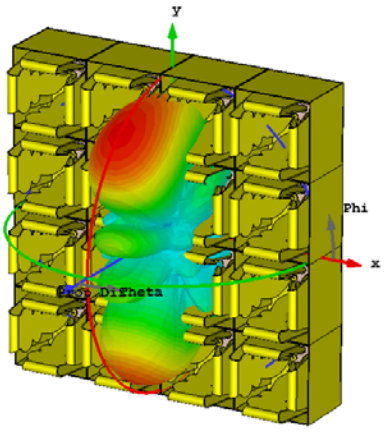

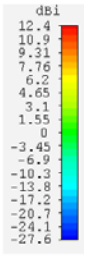

Type	Farfield
Approximation	enabled (kR >> 1)
Monitor	farfield (f=4.8) [SP_60_H]
Component	Abs
Output	Directivity
Frequency	4.8 GHz
Rad. effic.	-0.03157 dB
Tot. effic.	-1.016 dB
Dir.	12.41 dBi